

AFIT/GE/ENG/99M-19

**THE EFFECT OF REGISTRATION ERRORS
ON TRACKING IN A
NETWORKED RADAR SYSTEM**

THESIS

**Bradley John Mortenson
Captain, USAF**

AFIT/GE/ENG/99M-19

19990413 089

Approved for public release, distribution unlimited

REPORT DOCUMENTATION PAGE			Form Approved OMB No. 0704-0188	
Public reporting burden for this collection of information is estimated to average 1 hour per response, including the time for reviewing instructions, searching existing data sources, gathering and maintaining the data needed, and completing and reviewing the collection of information. Send comments regarding this burden estimate or any other aspect of this collection of information, including suggestions for reducing this burden, to Washington Headquarters Services, Directorate for Information Operations and Reports, 1215 Jefferson Davis Highway, Suite 1204, Arlington, VA 22202-4302, and to the Office of Management and Budget, Paperwork Reduction Project (0704-0188), Washington, DC 20503.				
1. AGENCY USE ONLY (Leave Blank)	2. REPORT DATE Mar 99	3. REPORT TYPE AND DATES COVERED Final		
4. TITLE AND SUBTITLE The Effect of Registration Errors on Tracking in a Networked Radar System		5. FUNDING NUMBERS		
6. AUTHORS Bradley J. Mortenson, Capt, USAF				
7. PERFORMING ORGANIZATION NAME(S) AND ADDRESS(ES) Air Force Institute of Technology 2950 P St Wright-Patterson AFB OH 45433-7765		8. PERFORMING ORGANIZATION REPORT NUMBER AFIT/GE/ENG/99M-19		
9. SPONSORING / MONITORING AGENCY NAME(S) AND ADDRESS(ES) Frederick N. Beaman, GS-13, Electronic Engineer, NAIC/TAER 4180 Watson Way Wright-Patterson AFB, OH 45433 (513) 257-4215		10. SPONSORING / MONITORING AGENCY REPORT NUMBER		
11. SUPPLEMENTARY NOTES Thesis Advisor: Dr. Steven C. Gustafson (513) 255-3636 ext. 4598 Steven.Gustafson@afit.af.mil				
12a. DISTRIBUTION / AVAILABILITY STATEMENT Approved for public release, distribution unlimited		12b. DISTRIBUTION CODE		
13. ABSTRACT (Maximum 200 words) To successfully combine information from distributed radar sensors, it is essential that each sensor be correctly referenced in a global coordinate system. If there are biases in the reported position of these sensors, the reported target position will also be biased and the ensuing global estimate of the target position will be degraded. Furthermore, any biases in range or azimuth measurements of these sensors will likewise be reflected in the degradation of global estimate of target position. Registration is the process of ensuring that these errors do not result in the creation of an additional redundant target when only a single target exists. The objective of this thesis is to create a model for analyzing the impact of these biases quantitatively. The model consists of modules which perform the required coordinate conversion, tracking, and data correlation. The target tracks are provided by a standard Kalman filter assuming a constant velocity model. The measurements, state estimates, and covariance matrices obtained from the Kalman filter are combined to form a Chi-squared correlation gate. With this model, the bounds on position, range, and azimuth biases are determined individually and cumulatively. The simulated results compare favorably with the theoretically determined bounds. An additional benefit of this model is that the spatial dependence of the biases may be obtained.				
14. SUBJECT TERMS Multiple sensor fusion Data correlation Networked Radar			15. NUMBER OF PAGES 90	
			16. PRICE CODE	
17. SECURITY CLASSIFICATION OF REPORT UNCLASSIFIED	18. SECURITY CLASSIFICATION OF THIS PAGE UNCLASSIFIED	19. SECURITY CLASSIFICATION OF ABSTRACT UNCLASSIFIED	20. LIMITATION OF ABSTRACT UL	

**THE EFFECT OF REGISTRATION ERRORS
ON TRACKING IN A
NETWORKED RADAR SYSTEM**

THESIS

Presented to the Faculty of the School of Engineering
Of the Air Force Institute of Technology
In Partial Fulfillment of the
Requirements for the Degree of
Master of Science in Electrical Engineering

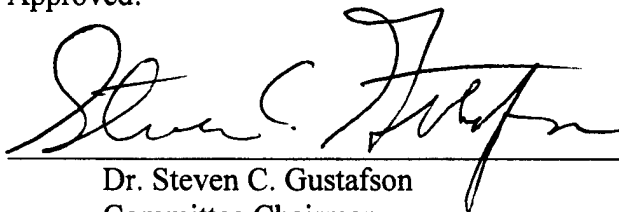
**Bradley John Mortenson, M.S.E.E.
Captain, USAF**

March 1999

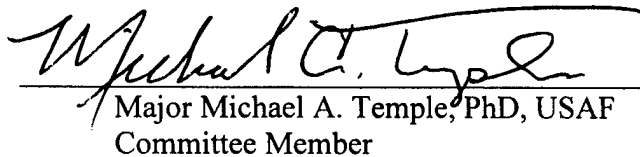
**THE EFFECT OF REGISTRATION ERRORS
ON TRACKING IN A
NETWORKED RADAR SYSTEM**

Bradley J. Mortenson, M.S.E.E.
Captain, USAF

Approved:


Dr. Steven C. Gustafson
Committee Chairman

3 March 1999
date


Major Michael A. Temple, PhD, USAF
Committee Member

3 Mar 99
date

Acknowledgments

I would like to thank my Thesis advisor Dr. Steven Gustafson, Thesis committee advisor Major (Dr.) Michael Temple, and my Thesis sponsor Mr. Frederick Beaman (NAIC/TAER, (Ground Radar)) who formulated this research topic, for their invaluable advice and patience in this effort.

Additionally, I would like to thank the numerous faculty and fellow students whom I have conferred with during the development of this Thesis. I would also like to thank all of the AFIT support personnel who have allowed me to focus on academic concerns instead of administrative issues.

TABLE OF CONTENTS

1. INTRODUCTION.....	1
1.1 BACKGROUND.....	2
1.2 RESEARCH MOTIVATION.....	3
1.3 SCOPE OF RESEARCH.....	4
1.4 DOCUMENT OVERVIEW.....	5
2. SUMMARY OF CURRENT KNOWLEDGE	6
2.1 RANDOM VERSUS SYSTEMATIC ERRORS	10
2.2 QUANTITATIVE REQUIREMENTS FOR REGISTRATION	12
2.3 ANALYSIS MODEL.....	14
2.4 QUANTITATIVE REQUIREMENTS.....	18
2.5 SUMMARY	24
3. SIMULATION MODEL DESCRIPTION	25
3.1 DEVELOPMENT OF THE SIMULATION MODEL	25
3.2 SIMULATION MODEL BLOCK DIAGRAM DESCRIPTION	26
3.3 ASSUMPTIONS	31
3.3.1 FIXED SAMPLE (OR MEASUREMENT) INTERVALS	31
3.3.2 SINGLE TARGET.....	31
3.3.3 NO CLUTTER / FALSE ALARMS.....	31
3.3.4 100 % PROBABILITY OF DETECTION	32
4. ANALYSIS OF RESULTS.....	33
4.1 OVERVIEW	33
4.2 POSITIONAL BIAS	35
4.3 RANGE BIAS	38
4.4 AZIMUTH BIAS	41
4.5 SIMULTANEOUS POSITION-RANGE-AZIMUTH BIASES	42
5. SUMMARY / RECOMMENDATIONS.....	45
5.1 COORDINATE TRANSFORMATIONS	45
5.2 KALMAN ALGORITHM.....	45
5.3 ANALYTICAL MODEL DEVELOPMENT	46
5.4 SYSTEM MODEL	46
5.5 BIAS EFFECTS.....	47
5.6 RECOMMENDATIONS	48
5.6.1 VECTORIZE THE KALMAN FILTER ALGORITHM	48
5.6.2 ACCEPT ASCII/MAT PLOT FILES	48
5.6.3 MULTIPLE RADARS	49
5.6.4 DEGRADATION OF TRACKING ACCURACY.....	49
5.6.5 THE EFFECT OF SAMPLE TIME	50
5.6.6 MULTIPLE-HYPOTHESIS TRACKING.....	50
1A. APPENDIX 1 KALMAN FILTERING INTRODUCTION	51
1A.1 LINEAR SYSTEM MODEL	51
1A.2 DISCRETE-TIME KALMAN FILTERING.....	53
2A. APPENDIX 2 DERIVATION OF KALMAN FILTER EQUATIONS	60

2A.1	FIRST DERIVATION:	60
2A.2	SECOND DERIVATION:	61
3A.	APPENDIX 3 LOCAL TO GLOBAL COORDINATE TRANSFORMATION.....	67
3A.1	THE TRANSLATION:	69
3A.2	FIRST ROTATION:	71
3A.3	SECOND ROTATION:	72
3A.4	THIRD ROTATION:	72
3A.5	MATLAB ROUTINES	73
4A.	APPENDIX 4 MODIFIED MUNKRES ALGORITHM.....	76
6.	LIST OF NOTATION / SYMBOLS.....	80
7.	BIBLIOGRAPHY	81
8.	VITA.....	82

TABLE OF FIGURES

Figure 2-1 Constant Measurement Error Ellipses	9
Figure 2-2 Non-central Chi-square (χ^2) cdf vs. non-centrality parameter.....	18
Table 2-1 Registration Error Budgets.....	24
Figure 3-1 Top-Level Block Diagram.....	26
Figure 3-2 Path Generation Block Diagram	27
Figure 3-3 Coordinate Conversion and Bias Insertion Block Diagram.....	27
Figure 3-4 Kalman Filter and Chi-square Gate Test Block Diagram	28
Figure 3-5 Kalman Filter State Estimation Loop	29
Figure 3-6 Kalman Filter Covariance and Kalman Gain Loop	29
Figure 3-7 Chi-Square Gate Test Block Diagram	30
Figure 4-1 Representative Constant-Error Ellipses.....	33
Figure 4-2 Constant-Error Ellipses vs. Target Position.....	34
Figure 4-3 Position Bias Target Path.....	35
Figure 4-4 Position Bias vs. Target Position	37
Figure 4-5 Position Bias 95% Confidence Level (one-sided) vs. Target Position	38
Figure 4-6 Range Bias Target Path	39
Figure 4-7 Range Bias vs. Target Position	40
Figure 4-8 95% Confidence Level Range bias vs. Target Position.....	40
Figure 4-9 Azimuth Bias vs. Target Position	41
Figure 4-10 95% Confidence Level of Azimuth Bias vs. Target Position	42
Figure 4-11 Simultaneous Position-Range-Azimuth Bias vs. Target Position.....	44
Figure 4-12 Position-Range-Azimuth 95% Confidence Level.....	44
Figure 3A-1 Target in two Radar System.....	67
Figure 3A-2 Transformation from Geographical to Geocentric Coordinates	68
Figure 3A-3 An Ellipse Description by the Slope of the Normal Vector.....	69
Figure 3A-4 Coordinate Transformation Diagram	70

ABSTRACT

To successfully combine information from distributed radar sensors, it is essential that each sensor be correctly referenced in a global coordinate system. If there are biases in the reported position of these sensors, the reported target position will also be biased and the ensuing global estimate of the target position will be degraded. Furthermore, any biases in range or azimuth measurements of these sensors will likewise be reflected in the degradation of global estimate of target position. Registration is the process of ensuring that these errors do not result in the creation of an additional redundant target when only a single target exists.

The objective of this thesis is to create a model for analyzing the impact of these biases quantitatively. The model consists of modules which perform the required coordinate conversion, tracking, and data correlation. The target tracks are provided by a standard Kalman filter assuming a constant velocity model. The measurements, state estimates, and covariance matrices obtained from the Kalman filter are combined to form a Chi-squared correlation gate. With this model, the bounds on position, range, and azimuth biases are determined individually and cumulatively. The simulated results compare favorably with the theoretically determined bounds. An additional benefit of this model is that the spatial dependence of the biases may be obtained.

THE EFFECT OF REGISTRATION ERRORS ON TRACKING IN A NETWORKED RADAR SYSTEM

1. Introduction

Air defense and air traffic control systems depend on a surveillance subsystem to provide an overall picture of the air situation in order to make decisions. To maintain an accurate, complete, and current air picture, the surveillance subsystem, in turn, depends on combinations of networked sensors to provide the raw data from which the picture is constructed.

The general registration problem arises whenever it is desired to combine information from two or more sensors into a single "system level" surveillance picture. The most important attribute of a "good" surveillance picture is that it contains exactly one track for each object detected by at least one sensor in the system. The fundamental problem in sensor networking, therefore, is to determine whether the data reported by two or more sensors represent a common object or two (or more) distinct objects.

There are often systematic errors which effectively introduce biases into the track estimation process. Therefore, failure to register adequately in a multiple radar system can result in varying degrees of performance degradation, depending on the magnitude of the biases with respect to the random measurement errors and the track correlation gates. The level of degradation ranges, at worst, from the formation of multiple redundant tracks for a single aircraft to reduced track accuracy and stability when the bias is relatively small. In between, the benefits of a multiple radar system can be negated and the system, in effect, can be reduced to a single radar tracking system[Bar90].

It should be noted that this topic is really a special case of a more general sensor fusion problem which may employ many diverse sensors. Data from different sensors and types of sensors are combined using techniques drawn from several disciplines, such as signal processing, statistics, artificial intelligence, pattern recognition, cognitive psychology, and information theory.

Sensor fusion is analogous to the cognitive process used by humans and other life forms to combine data from their senses and a priori knowledge to make inferences about the external world. One description of the hierarchy of sensor fusion inference ranges from lowest to the highest: existence of an entity, position/velocity determination, identity of signal sources, behavior of entities, situation assessment, and finally threat analysis as the highest level of inference[Hal92]. Thus, this paper addresses a relatively low-level sensor fusion inference process.

1.1 Background

A typical networked radar system consists of a collection of remotely located radars. Each radar provides a sequence of time-ordered measurements of position (r, θ) in polar coordinate system or (r, θ, ϕ) in spherical coordinates; in either case, the origin of the measurement coordinate system is located at the radar antenna. The basic detection processing, signal processing, and post-detection processing all occur at the radar site. The digitized position reports, often called plots, are forwarded to a central track processor over a digital data link. Accurate data registration is a prerequisite for satisfactory track initiation and plot-to-track correlation; improved registration reduces requirements for human-machine interfacing required to resolve initiation and correlation errors.

At the central tracking processor, plots from the multiple radars update existing system tracks or initiate new system tracks as appropriate. Specifically, the central tracking processor must perform the following functions:

1. Transformation of the radar plots from local radar coordinates to system, or global, coordinates.
2. Correlation or association of the radar plots with the appropriate system tracks. Because there are multiple radars in the system, more than one plot may correlate with the same track over some arbitrary time interval.
3. Initiation of new tracks with the uncorrelated plots and rejection of clutter plots.
4. Track filtering (or updating with correlated plots) and track prediction.
5. Track monitoring and system track management (including association with tracks from external sources).

Functions 2 and 4 represent the heart of the traditional data association and tracking problem. However, before either of these processes can occur successfully, function 1 must be performed; that is, the individual radar data must have a common coordinate system in which the errors due to site uncertainties, antenna orientation, and improper calibration of range and time are minimized so they do not cause a significant degradation of the system operation. The process of ensuring the required “error free” (or, more precisely, controlled error) coordinate conversion of radar data is called registration. Thus, registration is an absolute prerequisite for multiple radar tracking or sensor networking in general[Bar90].

1.2 Research Motivation

Electronic position location systems such as the global positioning system (GPS) or commercial satellite survey systems can locate a position on the earth’s surface to within a maximum error of about 30 meters[Bar90]. This accuracy seems adequate for radar systems where the standard deviation of the range measurement error is greater than 100 m. However, in the event of a degraded or absent GPS signal, a

mobile ground radar may have a positional error on the order of the range measurement error. This fact motivates our analysis of the specific effect of radar positional uncertainties (biases) on tracking errors.

The other systematic error sources addressed, the range and azimuth offsets (or biases), are determined in part by radar detection technique (Doppler, mono-pulse, etc.), oscillator (clock) stability and jitter, wind torque and mechanical imperfections (for a physically rotated antenna), and calibration or alignment imperfections, etc.. By examining the effect of the net position and range and azimuth offsets, a budget may be obtained that determines the allowable tolerance of each of the above error sources.

1.3 Scope of Research

Of the sources of registration error, three sources which have proven to be major problems in air defense and air traffic control systems are analyzed: (1) position of the radar with respect to the system coordinate origin; (2) alignment of the antennas with respect to a common North reference (that is, the azimuth offset); and (3) range offset errors. Other errors may exist in current radar systems; however, they have not been significant problems in the past[Bar90].

The fourth source of error, the inherent inability of 2D radars to produce the correct ground range for conversion to Cartesian coordinates, is not considered. This error is not random, it always results in an overestimate of the ground range; the magnitude of the error depends on the aircraft range and elevation angle. The only real solution to this problem is the use of 3D radars. Otherwise, the best that can be done is to include this error as a component of the range measurement error. To remove this source of error from our model, the target path is generated in three dimensions and the required translation and rotations are performed by approximating the Earth's geoid shape with an ellipsoid. See Appendix 2 for the development of these spatial transformations. The range and azimuth measurements are then extracted, effectively removing the ground range error.

1.4 Document Overview

Chapter two addresses pertinent requirements for determining adequate registration. First an analytic framework is developed to analyze this issue, with the Kalman filter model as the underlying structure. Background theory for the Kalman filter is included in Appendices one and two. With this analysis model, specific quantitative requirements for registration are then developed. Based on a Chi-square error distribution, bounds for the position, range, and azimuth errors are established.

Chapter three describes the development of the simulation model and provides block diagrams for each module. In addition, the operation of each module is described in detail and the associated assumptions are listed.

Chapter four provides the results of the simulations and the accompanying analysis. The target paths and representative error ellipse geometries are included to help visualize the results.

Chapter five provides a summary of this research effort and offers suggestions for further development.

2. Summary of Current Knowledge

To combine information from multiple sensors, radars in our case, a tracking algorithm is often implemented to provide measurement accuracies (or statistics). The word tracking implies that there exists a state estimate \mathbf{S}^* together with a covariance matrix \mathbf{P}^* for each detected aircraft. The pair $(\mathbf{S}^*, \mathbf{P}^*)$ could be obtained, for example, from the standard Kalman filter for a constant velocity plant model (that is, no acceleration). The Kalman filter used in this application is a four-state discrete-time filter. If not familiar with Kalman filters, refer to Appendices 1 and 2 for background information on Kalman filtering described in the context of tracking. While this paper is not intended to be a treatise on Kalman filtering, and definitely doesn't qualify as one, as will be seen, the Kalman filter provides the tracking error statistics necessary for the analysis of registration errors.

To associate observations with existing tracks, a track updating process typically begins with a gating procedure that is used to eliminate unlikely observation-to-track pairings. Processing is done at each scan using only data received on that scan to update the results of previous processing. This process assigns observations to existing tracks in a manner that minimizes some overall distance criterion. At scan $k-1$, the filter forms the prediction $\hat{\mathbf{S}}_{k|k-1}$ of the state vector for use at time kT . The measurement at scan k is $\mathbf{Z}_k = \mathbf{H} \cdot \mathbf{S}_k + \mathbf{V}_k$, where \mathbf{H} is the observation matrix and \mathbf{V} is zero-mean, white Gaussian measurement noise with covariance matrix \mathbf{R} . The vector difference between the measured and predicted quantities, $\mathbf{v}_k = \mathbf{Z}_k - \mathbf{H} \cdot \hat{\mathbf{S}}_{k|k-1}$, is defined as the residual, or innovation, with residual covariance matrix, $\mathbf{\Theta} = \mathbf{H} \cdot \mathbf{P} \cdot \mathbf{H}^T + \mathbf{R}$, where \mathbf{P} is the one-step prediction covariance matrix. The time subscripts will now be dropped for notational convenience. Assume that the measurement is of dimension M . Then defining d^2 to be the norm of the residual (or innovation) vector, $d^2 \equiv \mathbf{v}^T \cdot \mathbf{\Theta}^{-1} \cdot \mathbf{v}$, the M -dimensional Gaussian probability density function for the residual is

$$f(\nu) = \frac{e^{-\frac{d^2}{2}}}{(2\pi)^{M/2} \sqrt{|\Theta|}} \quad (2.1)$$

where $|\Theta| \equiv$ the determinant of Θ [Bla86].

In either of the special cases where the probability of detection is unity or there are no expected extraneous returns, the gate size should be infinite for optimal correlation performance. However, since one of the primary purposes of gating logic is to reduce the number of observation-to-track pairings that must be considered, a finite gate size would be appropriate even in these cases. Also, for non-unity probability of detection or during the presence of extraneous returns, an optimal, non-infinite gate size can be defined.

Since d^2 is the sum of squares of M independent Gaussian random variables, it has by definition a Chi-square (χ^2) distribution, thus a correlation gate (G) can be defined such that the plot-to-track association or correlation decision is based on a Chi-squared test of the following form:

$$[\hat{\mathbf{S}}_p - \mathbf{Z}]^T [\hat{\mathbf{P}}_p + \mathbf{P}_z]^{-1} [\hat{\mathbf{S}}_p - \mathbf{Z}] < G \quad (2.2)$$

where $\hat{\mathbf{S}}_p$ denotes the position components of \mathbf{S}^* extrapolated to the time at which the next measurement \mathbf{Z} is obtained; that is,

$$\hat{\mathbf{S}} = \Phi(\Delta t) \mathbf{S}^* \quad \hat{\mathbf{P}} = \Phi(\Delta t) \mathbf{P}^* \Phi(\Delta t)^T \quad (2.3)$$

where $\Phi(\Delta t)$ is the state transition matrix for a time Δt . Also \mathbf{Z} is the measured position (in 2D Cartesian coordinates), $\hat{\mathbf{P}}_p$ the covariance submatrix of $\hat{\mathbf{P}}$ for the position components, and $\hat{\mathbf{P}}_z$ the covariance matrix for the measurement.

If a radar measurement \mathbf{Z} from radar A satisfies the gate test defined by (2.2), then \mathbf{Z} is used to update the track through the estimation procedure. If more than one measurement from radar A satisfies the gate test, then an ambiguity resolution logic is necessary to select one measurement for the track update process. This can be accomplished with an optimal assignment algorithm such as the Munkres algorithm. However, if no measurement from radar A satisfies the gate test, then the gate G may be enlarged by adding a “maneuver term”:

$$G' = G + (1/C)(\Delta M)^2, \Delta M = At^2/2 \quad (2.4)$$

for a maneuver or acceleration factor A . The normalizing factor C can be defined as either the minimum eigenvalue of the joint covariance matrix $[\mathbf{P}_p + \mathbf{P}_z]$ or the n^{th} root of the determinant of the $(n \times n)$ covariance matrix. If the correlated plot is in the maneuver gate (but not in the nonmaneuver gate) for two or more successive scans, then a “maneuver” might be declared and a special set of maneuver gains or filter constants used to update the track. A maneuver gate is not implemented in the model since only linear target paths are generated. This is done to simplify the Kalman filter algorithm. The Kalman filter is the optimal estimator for a linear path, however a maneuvering target requires an extended Kalman filter in which its state vector is augmented with additional components.

Referring to Figure 2-1, suppose that an aircraft is tracked by two radars denoted as radars A and B whose detectable coverage areas overlap. Where, or even if, a plot from radar B falls in the correlation gates depends both on the random measurement errors of the radar and the magnitude of the position, range, and azimuth biases between the two radars.

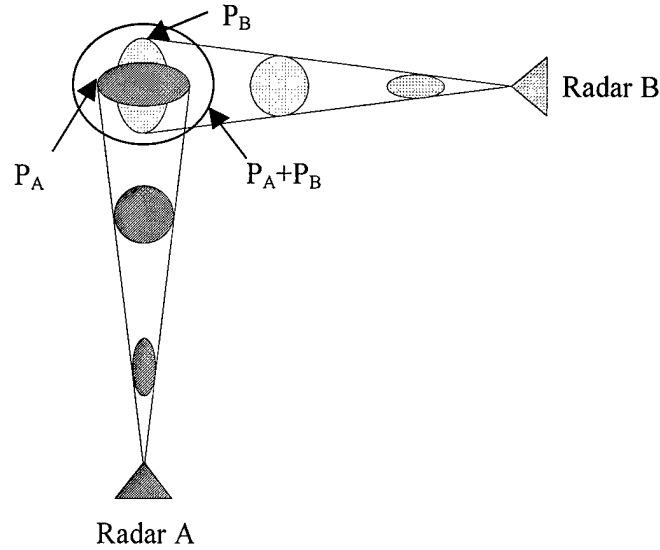


Figure 2-1 Constant Measurement Error Ellipses

If there are no registration errors or biases, then the plot from radar B should fall within the nonmaneuver gate G most of the time. Presumably, gate G was chosen to ensure that plots from a nonmaneuvering aircraft will satisfy (2.2) with a probability in the range 0.90 to 0.99, based on the characteristics of the random errors and the actual system design goals. Similarly, if the biases are small with respect to the random errors, then the plot from radar B should be in the nonmaneuver gate most of the time, although the exact probability will be less than the design goal. Similarly, if the biases are small with respect to the random errors, then the plot from radar B should be in the nonmaneuver gate most of the time, although the exact probability will be less than the design goal.

On the other hand, if the biases are relatively large with respect to the random errors, perhaps approximately of the size of the gate G or even G' , then the plot may fall between the nonmaneuver and the maneuver gates:

$$G \leq [\hat{\mathbf{S}}_p - \mathbf{Z}]^T [\hat{\mathbf{P}}_p + \mathbf{P}_Z]^{-1} [\hat{\mathbf{S}}_p - \mathbf{Z}] < G' \quad (2.5)$$

Although it is unlikely that a tracking system would be designed to declare a maneuver on one maneuver gate correlation, the possibility now exists that a maneuver could be falsely declared if radar A subsequently fails to detect the aircraft on the next scan. If the plot from radar B is used to update the track, then the bias is superimposed on the state estimate, with a loss of system track accuracy. If the plot is simply discarded, then the system may have a delayed response to an actual aircraft maneuver; certainly, there is a loss of information. Finally, if the biases are very large with respect to the random errors, then the plot from radar B will not correlate with the track at all, in which case the system eventually will initiate a second track for the same aircraft.

2.1 Random versus Systematic Errors

It was asserted in the preceding paragraph that the biases or registration errors in plot data would degrade system track accuracy if used to update a system track. However, this is only one example of a more general problem in the general theory of estimation. To consider the more general problem, let X be a random variable with an expected value μ and standard deviation σ ; that is,

$$\mu = E[X], \sigma^2 = E[(X - \mu)^2] \quad (2.6)$$

A random sample x from X can be represented as

$$x = \mu + \varepsilon \quad (2.7)$$

where ε is the zero-mean random component of X ; therefore,

$$E[\varepsilon] = 0, \sigma^2 = E[\varepsilon^2] \quad (2.8)$$

In many radar tracker designs, it is assumed that the radar measurements have the properties just outlined. In particular, it is assumed that μ represents the true value of the aircraft position. Tracking or filtering is a process for estimating the true aircraft position μ from a sequence of measurements; that is,

random samples, taken over time. Thus, if the set of measurements $\{x_1, x_2, x_3, \dots, x_N\}$ is available; then the estimate x^* of μ is given by

$$X^* = a_1x_1 + a_2x_2 + a_3x_3 + \dots + a_Nx_N \quad (2.9)$$

where the set of nonnegative scalars $\{a_1, a_2, a_3, \dots, a_N\}$, determined by the gains of the filter algorithm, satisfies the usual convexity criterion:

$$a_1 + a_2 + a_3 + \dots + a_N = 1 \quad (2.10)$$

If it is true that $E[\varepsilon] = 0$, then x^* is an unbiased estimate of the true position μ of the aircraft.

However, if $E[\varepsilon] = \beta$, where β is not zero ($\beta \neq 0$), then by (2.10) it follows that

$$E[x^*] = \mu + \beta \quad (2.11)$$

and the estimate x^* is a biased estimate of μ . Moreover, the mean square error (mse), V , of a biased estimate of x^* is larger than an unbiased estimate; that is,

$$V[x^*] = E[(x^* - \mu)^2] = (a_1^2 + a_2^2 + a_3^2 + \dots + a_N^2)\sigma^2 \quad (2.12)$$

if $E[\varepsilon] = 0$; whereas

$$V[x^*] = E[(x^* - \mu)^2] = (a_1^2 + a_2^2 + a_3^2 + \dots + a_N^2)\sigma^2 + \beta^2 \quad (2.13)$$

if $E[\varepsilon] = \beta$.

From this it follows that the process of filtering or state estimation “averages” the random measurement errors to reduce the variance or mse of the estimate of the true state μ . However, the filtering process cannot remove or even reduce the magnitude of the bias or systematic errors.

In the context of a multiple radar tracking system, the presence of registration errors will result in a track mse larger than that which should be achievable theoretically. If the registration errors are sufficiently large, then multiple radar tracking will be less accurate than single radar tracking. In the worst case, registration errors can result in a failure to correlate multiple radar measurements from a common aircraft with a common track, either reducing the system effectively to a single radar system or even leading to multiple tracks for the same aircraft. Because the fundamental objective of multiple radar tracking is to ensure track continuity for an aircraft as it moves through multiple radar coverage envelopes, registration errors can defeat the very purpose of a multiple radar system. Therefore, the basic requirement for registration is to ensure that plots, that is, radar measurements, from a common aircraft will be in the nonmaneuver correlation gate (in the absence of maneuvers)[Bar90].

2.2 Quantitative Requirements for Registration

At this point, the need for radar registration should be obvious. The next question therefore is, how well must radars be registered? Before it will be possible to address this question directly, some results from the distribution theory for normally distributed random variables must be stated. Based on this theory, an analysis model for the effects of registration errors on plot correlation will be developed. Finally, this model will be applied to derive some quantitative requirements for the three major sources of registration error: sensor position, range offset, and azimuth offset. These results are discussed at length in many textbooks on multivariate statistical analysis.

For this discussion, assume that $\{X_k \mid k = 1, 2, \dots, N\}$ is a set of normally distributed, scalar random variables with

$$E[X_k] = \mu_k, \quad E[(X_k - \mu_k)^2] = \sigma_k^2 \quad (2.14)$$

that is, each X_k is distributed as a $N(\mu_k, \sigma_k)$ random variable.

Now consider a random variable Z defined as the normalized sum of squares of the X_k :

$$Z = \sum_{k=1}^N \left(\frac{X_k - \mu_k}{\sigma_k} \right)^2 \quad (2.15)$$

The random variable Z is distributed as a Chi-squared random variable with N degrees of freedom, denoted by $\chi^2(N)$. The distribution $\chi^2(N)$ is often called the central Chi-squared distribution because each of the normalized terms,

$$X'_k = \frac{X_k - \mu_k}{\sigma_k} \quad (2.16)$$

from the sum of (2.15) is distributed as a $N(0, 1)$ random variable, which is often noted $X'_k \sim N(0,1)$.

Equivalently, each normalized term squared

$$Z_k = (X'_k)^2 = \left(\frac{X_k - \mu_k}{\sigma_k} \right)^2 \quad (2.17)$$

is a $\chi^2(1)$ random variable. If the means μ_k are omitted from the sum in (2.15), that is,

$$Z = \sum_{k=1}^N \left(\frac{X_k}{\sigma_k} \right)^2 \quad (2.18)$$

then Z is distributed as a noncentral Chi-squared random variable with parameter λ , denoted by $Z \sim \chi^2(N, \lambda)$. The noncentrality parameter λ is defined

$$\lambda = \sum_{k=1}^N \left(\frac{\mu_k}{\sigma_k} \right)^2 \quad (2.19)$$

The general theory just outlined can be extended to random vectors in a straightforward manner. For this case, let \mathbf{X} denote a normally distributed random vector in \mathbf{R}^N with mean $\boldsymbol{\mu}$ and covariance matrix \mathbf{P} . Then the quadratic form ξ defined by

$$\xi = (\mathbf{X} - \boldsymbol{\mu})^T \mathbf{P}^{-1} (\mathbf{X} - \boldsymbol{\mu}) \quad (2.20)$$

is distributed as a $\chi^2(N)$ random variable, $\xi \sim \chi^2(N)$. Similarly, if the quadratic form ξ is defined

$$\xi = \mathbf{X}^T \mathbf{P}^{-1} \mathbf{X} \quad (2.21)$$

then, $\xi \sim \chi^2(N, \lambda)$, where the noncentrality parameter λ is given by

$$\lambda = \boldsymbol{\mu}^T \mathbf{P}^{-1} \boldsymbol{\mu} \quad (2.22)$$

2.3 Analysis Model

With the help of the general theory just outlined, it is now possible to develop a mathematical model with which the quantitative effects of registration errors can be examined, specifically, the effects on multiple radar tracking and correlation. To proceed, let \mathbf{Z} denote a measurement of an aircraft position from a radar in the system. We assume that tracking is performed in a Cartesian coordinate system, either \mathbf{R}^4 or \mathbf{R}^6 , (the positions x, y or x, y, z and their corresponding velocities). Consequently, it may be assumed that \mathbf{Z} is in system coordinates; that is, the measurement vector \mathbf{Z} is of the form $[x, y]$ or $[x, y, z]$, rather than the natural radar polar coordinates $[r, \theta]$ or $[r, \theta, \phi]$.

Although it cannot be proven rigorously, we may assume that the measurement \mathbf{Z} is a normally distributed random vector with the mean equal to the true aircraft position. This assumption is partially justified for two reasons. First, the radar range measurement r generally follows a Rayleigh distribution. The azimuth measurement θ certainly is not uniformly distributed over the interval $[0, 2\pi)$; however the value of the azimuth, in effect, is quantized in the radar signal processor and in the analog-to-digital conversion process. Consequently, it is reasonable to assume that θ is approximately uniformly distributed over some subinterval of $[0, 2\pi)$ [Bar90]. It can be shown that the polar-to-Cartesian coordinate conversion

$$x = r \cos(\theta), \quad y = r \sin(\theta) \quad (2.23)$$

yields two independent $N(0, 1)$ random variables if r follows a Rayleigh distribution and θ is uniformly distributed over $[0, 2\pi]$ [Pap91].

If the random variables x and y are $\sim N(0, \sigma)$ and independent,

$$f_{XY}(x, y) = \frac{1}{2\pi\sigma^2} e^{-(x^2+y^2)/2\sigma^2} \quad (2.24)$$

then to find the probability distribution function in polar coordinates,

$$f_{R\Theta}(r, \theta) = \frac{f_{XY}(x, y)}{|J(x, y)|} \quad (2.25)$$

where $|J(x, y)|$ is the absolute value of the Jacobian of the polar to Cartesian transformation which is,

$$J(x, y) = \begin{vmatrix} \frac{\partial r}{\partial x} & \frac{\partial r}{\partial y} \\ \frac{\partial \theta}{\partial x} & \frac{\partial \theta}{\partial y} \end{vmatrix} = \begin{vmatrix} \frac{\partial x}{\partial r} & \frac{\partial x}{\partial \theta} \\ \frac{\partial y}{\partial r} & \frac{\partial y}{\partial \theta} \end{vmatrix}^{-1} = \begin{vmatrix} \cos \theta & -r \sin \theta \\ \sin \theta & r \cos \theta \end{vmatrix}^{-1} = \frac{1}{r} \quad (2.26)$$

where $|\cdot|$ is the determinant of the matrix. From (2.24), it can be concluded that,

$$f_{R\Theta}(r, \theta) = r \cdot f_{XY}(x, y) = \frac{r}{2\pi\sigma^2} e^{-r^2/2\sigma^2}, r > 0, |\theta| < \pi \quad (2.27)$$

and 0 otherwise. This is a product of a function of r times a function of θ . Hence the random variables r and θ are independent with

$$f_R(r) = \frac{r}{\sigma^2} e^{-r^2/2\sigma^2}, f_\Theta(\theta) = \frac{1}{2\pi}, r > 0, |\theta| < \pi \quad (2.28)$$

Where the proportionality constant is chosen to make the area (total probability) of each term equal to 1. Thus it follows that if x and y are $\sim N(0, \sigma)$ and independent, the random variables r and θ are independent with r being Rayleigh distributed and θ being uniformly distributed.

Secondly, empirical measurements gathered by Hughes Aircraft Company over past years suggests that the random errors in \mathbf{Z} are at least approximately normally distributed[Bar90]. It is true, however, that there is a distinct correlation in the errors between x and y . This is the reason for employing a Kalman filter capable of tracking in two dimensions. This allows us to take advantage of the coupling, or correlation, of the x and y measurements. Recall that the actual radar measurements are in polar coordinates, and any change in range or azimuth generally results in a corresponding change in x and y . Of course, in the special case of a target path co-linear with either the x or y axis, a change of range will not result in changes in both x and y .

Assume that a time-ordered sequence of correlated measurements $\{\mathbf{Z}_1, \mathbf{Z}_2, \mathbf{Z}_3, \dots, \mathbf{Z}_k\}$ are processed by a Kalman filter to obtain a track, which consists of a state estimate \mathbf{S}^* and a covariance matrix \mathbf{P}^* for the state estimate. Therefore, the state estimate \mathbf{S}^* is a linear combination of the measurements $\{\mathbf{Z}_1, \mathbf{Z}_2, \mathbf{Z}_3, \dots, \mathbf{Z}_k\}$. With the assumption of normality for the errors in \mathbf{Z} , and the natural assumption of independence of the time sequence of measurements, it follows that the state estimate \mathbf{S}^* is a normally distributed random vector.

Now consider the correlation criterion given in (2.2)

$$\xi = [\hat{\mathbf{S}}_p - \mathbf{Z}_{k+1}]^T [\hat{\mathbf{P}}_p + \mathbf{P}_Z]^{-1} [\hat{\mathbf{S}}_p - \mathbf{Z}_{k+1}] < G \quad (2.29)$$

The quadratic form ξ in (2.24) is distributed as a $\chi^2(M, \lambda)$ random variable with the number of degrees of freedom M equal to the dimension of the measurement vector \mathbf{Z} .

In theory, the non-centrality parameter λ should be zero if the measurement \mathbf{Z}_{k+1} was obtained from the same aircraft represented by the track vector \mathbf{S}^* . The parameter λ can be other than zero if either (1) the measurement \mathbf{Z}_{k+1} was obtained from a different aircraft than that represented by the track or (2) there are biases that would create an apparent difference without the random measurement errors. For this application, λ will represent the total normalized biases in the measurement vector \mathbf{Z} ; that is,

$$\lambda = \mathbf{b}^T [\hat{\mathbf{P}}_p + \mathbf{P}_z]^{-1} \mathbf{b} \quad (2.30)$$

Note that (2.25) assumes that the measurement vector \mathbf{Z} is of the form

$$\mathbf{Z} = \boldsymbol{\mu} + \mathbf{b} + \boldsymbol{\varepsilon} \quad (2.31)$$

where $\boldsymbol{\mu}$ is the true aircraft position and $\boldsymbol{\varepsilon}$ is the vector of random errors. Assuming that the mean of the prediction $\hat{\mathbf{S}}_p$ is $\boldsymbol{\mu}$, then

$$E[\hat{\mathbf{S}}_p - \mathbf{Z}] = \mathbf{b} \quad (2.32)$$

Equations (2.29) and (2.30) are the model with which the impact of registration errors can be analyzed quantitatively. The non-maneuver gate G and the maneuver gate G' are chosen to obtain a specified probability of correlation of plots that represent the same aircraft as the track. For example, G is chosen from a $\chi^2(M)$ probability distribution to satisfy

$$\text{Prob}[\xi < G] \geq p_0 \quad (2.33)$$

The objective now is to define an error “budget” for the sources of registration error such that

$$\text{Prob}[\xi < G] \geq p_0 - \Delta p \quad (2.34)$$

where the correlation statistic ξ is distributed as a $\chi^2(M, \lambda)$ random variable with parameter λ given by (2.30), and $\Delta p > 0$ is the reduction in the correlation probability that can be tolerated if the system still is to meet the system-level requirements for tracking or track accuracy.

2.4 Quantitative Requirements

To develop some specific requirements for registration, consider first the correlation gate size G . One common rule of thumb in tracking systems is to choose G such that

$$\text{Prob}[\xi < G] = 0.99 \quad (2.35)$$

If the measurement vector \mathbf{Z} is in \mathbf{R}^2 , then the inverse Chi-square with $N = 2$ degrees of freedom and a probability of .99 yields $G = 9.2$; similarly for \mathbf{Z} in \mathbf{R}^3 , $G = 11.3$. A correlation probability of 0.99 may be an excessive requirement considering the probability of detection of many surveillance radars, which often are specified to be only 0.8 to 0.9[Bar90]. Consequently, a correlation probability of 0.95 would seem adequate for most applications. Given that 0.95 is adequate, then from Figure 2-2, a gate size of 9.2 allows a total bias parameter $\lambda = 1.2$ for the two-dimensional case or $\lambda = 1.5$ for the three-dimensional case.

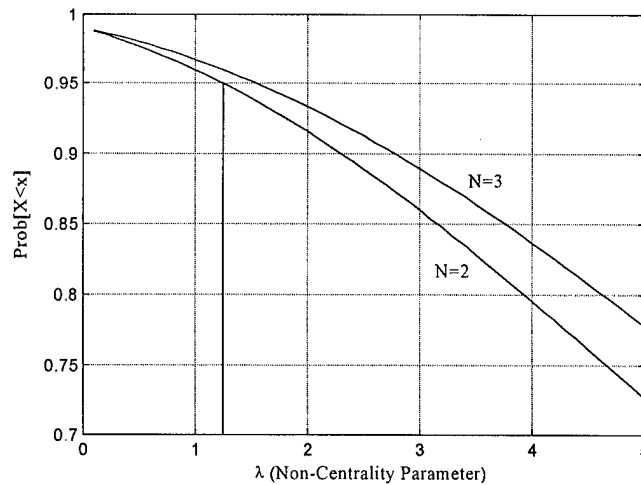


Figure 2-2 Non-central Chi-square (χ^2) cdf vs. non-centrality parameter

The three major sources of registration error are sensor position, range offset, and azimuth offset. The next step in the analysis, therefore, is to find the maximum error in each variable consistent with the bound of the parameter λ . In the following discussion, only the case of a two-dimensional measurement vector will be considered since the model's measurements are in those dimensions.

Consider an aircraft tracked by radars A and B. For convenience, let \mathbf{P}_A and \mathbf{P}_B denote the covariance matrices for the measurement errors at radars A and B, respectively. The registration problem is to ensure that the bias vector \mathbf{b} is sufficiently small that the measurement from radar B will correlate in the non-maneuver gate with the system track.

That is, the problem now is to bound the errors that contribute to the bias vector \mathbf{b} from the inequality

$$\mathbf{b}^T [\hat{\mathbf{P}}_P + \mathbf{P}_Z]^{-1} \mathbf{b} < 1.2 \quad (2.36)$$

Obviously, it would be convenient to eliminate one of the variance parameters. Many tracking systems, in an attempt to maintain sensitivity to possible aircraft maneuvers, bound the gains in the Kalman filter from below [Bar90]. One rule of thumb is to allow the gains to decrease to the level that produces steady state position variances to be approximately 50 percent of the corresponding measurement variances. Thus, (2.36) becomes

$$\mathbf{b}^T [0.5 \cdot \mathbf{P}_A + \mathbf{P}_B]^{-1} \mathbf{b} < 1.2 \quad (2.37)$$

Before continuing further, consider briefly the nature of the radar measurement error. In the radar measurement plane, that is, the $[r, \theta]$ plane, the covariance matrix \mathbf{P} is defined

$$\mathbf{P}'_R = \begin{pmatrix} \sigma_r^2 & 0 \\ 0 & r^2 \sigma_\theta^2 \end{pmatrix} \quad (2.38)$$

where σ_r and σ_θ are the standard deviations of the range and azimuth measurements, respectively; and where r is the range from the radar to the aircraft. In modern surveillance radars, the range measurement often is much more accurate than the cross-range measurement, which can result in highly elliptical equal-probability contours (or error ellipses) in the plane. The error ellipses in \mathbf{R}^2 have major and minor semi-axes equal to the square roots of the two diagonal components of the matrix in equation (2.38).

The basic concept of an error ellipse describes the eccentricity of a single radar error contour determined by the ratio of the range error σ_r to the cross-range error $r \cdot \sigma_\theta$. In this example, the range error σ_r is smaller than the cross-range error $r \cdot \sigma_\theta$, which creates highly elliptical errors in the plane for both radars. In Figure 2-1, the sum is nearly circular because of the orthogonal geometry of the aircraft and the two radars.

The conversion from radar coordinates to the Cartesian plane rotates an error ellipse in the plane by a unitary matrix of the form

$$\mathbf{U} = \begin{pmatrix} \cos \theta & -\sin \theta \\ \sin \theta & \cos \theta \end{pmatrix} \quad (2.39)$$

where θ is the angle to the target, measured counterclockwise from the abscissa, (the x axis), of the radar coordinate system. Thus,

$$\mathbf{P}_R = \mathbf{U} \cdot \mathbf{P}'_R \cdot \mathbf{U}^T \quad (2.40)$$

for radar R . Note that the unitary transformation \mathbf{U} merely rotates an error ellipse with respect to the axes of the Cartesian plane; it does not change the basic shape or area of an error ellipse. Because the angle θ will be different for different radars viewing the same aircraft, the orientation of the error ellipses \mathbf{P}_A and \mathbf{P}_B can be quite different, even if the error matrices \mathbf{P}'_A and \mathbf{P}'_B in the respective radar planes are similar.

Now, consider the problem of a bias \mathbf{b} due to an error in the knowledge of the position of radar B with respect to radar A. Equation (2.37) bounds the magnitude of \mathbf{b} relative to the sum of the tracking and measurement error variances $[0.5 \cdot \mathbf{P}_A + \mathbf{P}_B]$. The worst case geometry occurs when (1) the aircraft under consideration is at the midpoint of the line segment that joins the two radar locations and (2) the bias vector \mathbf{b} is parallel to that line.

$$\mathbf{b}^2 = |\mathbf{b}^T \mathbf{b}| < 1.8 \cdot \min[\sigma_r^2(A), \sigma_r^2(B)] = 1.8 \cdot \sigma_r^2(\min) \quad (2.41)$$

Now the limit of the allowable absolute position bias is defined as,

$$|\mathbf{b}_p| = 1.34 \cdot \sigma_r(\min) \quad (2.42)$$

This assumes, of course, that the range error is no greater than the cross-range error. However if this is not the case, then the cross-range error for some minimum detection range could be used instead. In this case, (2.37) becomes,

$$\mathbf{b}^2 = |\mathbf{b}^T \mathbf{b}| < 1.8 \cdot \min[r^2 \cdot \sigma_\theta^2(A), r^2 \cdot \sigma_\theta^2(B)] = 1.8 \cdot r^2 \sigma_\theta^2(\min) \quad (2.43)$$

where $\sigma_\theta(A)$ denotes the standard deviation of the azimuth measurements from radar A, and r is the down-range distance from the radar to the target. Therefore, taking the square root of equation (2.43) gives the maximum tolerance \mathbf{b}_p on the magnitude of the position error,

$$|\mathbf{b}_p| = 1.34 \cdot r \cdot \sigma_\theta(\min) \quad (2.44)$$

where $\sigma_\theta(\min)$ is the standard deviation of the radar with the smallest azimuth measurement error.

Next, consider the problem of range offset errors. The worst case geometry is the same as that for radar position errors. The range bias problem, however, is not a relative problem; that is, each radar can contribute an error. Whether these errors are additive or partially cancel each other depends on the exact

geometry as well as the sign of the bias. For the geometry under consideration, the worst case is for errors of the same sign. Therefore, the equivalent form of (2.44) is the following:

$$|2\mathbf{b}_R| = 1.34 \cdot \sigma_r(\min) \quad (2.45)$$

where \mathbf{b}_R is the maximum tolerance for the range bias at each radar; or equivalently,

$$|\mathbf{b}_R| = 0.67 \cdot \sigma_r(\min) \quad (2.46)$$

Lastly, consider the problem of antenna alignment or azimuth offset errors. The error or offset \mathbf{b} of the measurement from radar B will be parallel to the cross-range error (due to azimuth measurement errors). The magnitude of the error, b_θ , is given by

$$b_\theta = r_B(\Delta\beta_\theta) \quad (2.47)$$

where $\Delta\beta_\theta$ is the azimuth offset.

The geometry in this case is more complex; however, some empirical observations will suffice to show that the worst case occurs for an orthogonal aircraft-radar geometry. Assuming that the axes of the Cartesian coordinate system are aligned so that the origin, aircraft, and the two radars compose the four corners of a rectangle. The azimuth offset error will be along the cross-range error with respect to radar B, which is parallel to the range error for radar A. Therefore, it follows that

$$b_\theta^2 = |\mathbf{b}^T \mathbf{b}| < 1.2 \cdot [0.5 \cdot \sigma_r^2(A) + r^2 \cdot \sigma_\theta^2(B)] \quad (2.48)$$

If it is assumed that $\sigma_r(A) \ll r\sigma_\theta(B)$, then it follows that a reasonable bound for the azimuth offset $\Delta\beta_\theta$ is given by

$$|\Delta\beta_\theta| < 1.1 \cdot \sigma_\theta \quad (2.49)$$

Here, the azimuth offset has been treated as a relative error at radar B, which is adequate for a system of only two radars.

However, if the down-range measurement variance σ_r is greater than the cross-range measurement variance $r \cdot \sigma_\theta$, then

$$b_\theta^2 = |\mathbf{b}^T \mathbf{b}| < 1.2 \cdot [5 \cdot r^2 \cdot \sigma_\theta^2(A) + r^2 \cdot \sigma_\theta^2(B)] \quad (2.50)$$

and using equation (2.47) and the fact that the worst-case geometry will now occur when the target is centered between the two radars, and assuming the two azimuth variances are equal,

$$|\Delta\beta_\theta| < \sqrt{1.2} \cdot \sqrt{\frac{3}{2}} \cdot \sigma_\theta \cong 1.34 \cdot \sigma_\theta \quad (2.51)$$

which is about 22 % greater than the maximum allowable bias using the previous assumption.

In a system with three or more radars, it would be necessary to align each radar with respect to true north. Therefore, the actual requirement in a multiple radar system using the assumption that the cross-range measurement variance is much greater than the down-range variance is

$$|\Delta\beta_\theta| < 0.55 \cdot \sigma_\theta \quad (2.52)$$

Assuming the down-range variance is greater than the cross-range variance,

$$|\Delta\beta_\theta| < 0.67 \cdot \sigma_\theta \quad (2.53)$$

The results of these single-source error analyses are summarized in Table 1 in the form of a registration error budget. However, in actuality, these errors occur simultaneously, resulting in a cumulative error. If all three error sources are considered together as additive vectors, then by the nature

of vector addition, the error budget must be reduced by a factor of $\sqrt{3}$; the result is shown in the right-hand column of Table 2.1.

Table 2-1 Registration Error Budgets

Error Source	Single-Source Tolerance	Multi-Source Tolerance
Radar Position	$1.34 \cdot \sigma_r(\min)$ $\sigma_r(A) \ll r \cdot \sigma_\theta(B)$	$0.77 \cdot \sigma_r(\min)$ $\sigma_r(A) \ll r \cdot \sigma_\theta(B)$
	$1.34 \cdot r \cdot \sigma_\theta(\min)$ $\sigma_r(A) \approx r \cdot \sigma_\theta(B)$	$0.77 \cdot r \cdot \sigma_\theta(\min)$ $\sigma_r(A) \approx r \cdot \sigma_\theta(B)$
Range offset	$0.67 \cdot \sigma_r(\min)$	$0.39 \cdot \sigma_r(\min)$
Azimuth offset	$0.55 \cdot \sigma_\theta$ $\sigma_r(A) \ll r \cdot \sigma_\theta(B)$	$0.32 \cdot \sigma_\theta$ $\sigma_r(A) \ll r \cdot \sigma_\theta(B)$
	$0.67 \cdot \sigma_\theta$ $\sigma_r(A) \approx r \cdot \sigma_\theta(B)$	$0.39 \cdot \sigma_\theta$ $\sigma_r(A) \approx r \cdot \sigma_\theta(B)$

Note: $\sigma_r(\min)$ is the minimum standard deviation over all radars in the system. The bound for the azimuth bias can be taken relative to each site.

2.5 Summary

Developed in this chapter, is the model by which the effects of registration error in a networked radar system may be quantitatively analyzed. Also introduced is the concept of a correlation gate as the sum of squared Gaussian distributed random variables, constituting a non-central Chi-squared random variable with degrees of freedom, N equal to the number of dimensions in the measurement vector. It is observed that the correlation gates most often take the form of “error ellipses” in two-dimensional measurement space. Finally, the worst-case geometries for the target, radars and global coordinate origin are presented. The three sources of error considered, the position, range, and the azimuth biases are to be quantitatively analyzed individually and cumulatively.

3. Simulation Model Description

3.1 Development of the Simulation Model

One of the goals of this effort is the creation of a user-friendly software model which may be used in further analysis of networked radar systems. Since there exists a number of industry accepted and validated software models to simulate various radar types, resources are not expended in duplicating this capability. In addition, future efforts will be made to import radar plots generated from other tools as the input to this model. A model is desired that will be easily altered to allow for the analysis of differing sensor measurement characteristics, including azimuth and range measurement variances. It is also desirable to permit arbitrary placement of sensor positions, and to change the position, range, and azimuth biases easily.

Because of these desired characteristics, it is decided to implement the model in the graphical simulation environment Simulink[®], an extension to the widely accepted commercial software package MatLab[®]. One implication of using Simulink[®] is that not all MatLab[®] functions are directly callable from its block diagram simulation environment. To access certain MatLab[®] functions, or custom written functions, S-functions must be written. S-functions use a special calling syntax that enable you to interact with the MatLab[®] ordinary differential equation solver.

Another difficulty using Simulink[®] is that $(m \times n)$ matrices are decomposed and reconstructed into $(m \cdot n \times 1)$ vectors and passed from block-to-block during a simulation. To perform matrix calculations, it is advantageous to use the MatLab[®] Digital Signal Processing Blockset[®] to ease the burden of resizing these vectors into their original dimensions.

Despite these restrictions, Simulink® provides an intuitive environment for model creation, allows easy model parameter changes, and allows Monte-Carlo simulations to be performed from the MatLab® command line.

3.2 Simulation Model Block Diagram Description

The block diagrams that constitute the simulation model are now considered. Note that in the following illustrations, thicker lines denote vectors and the thinner lines scalars.

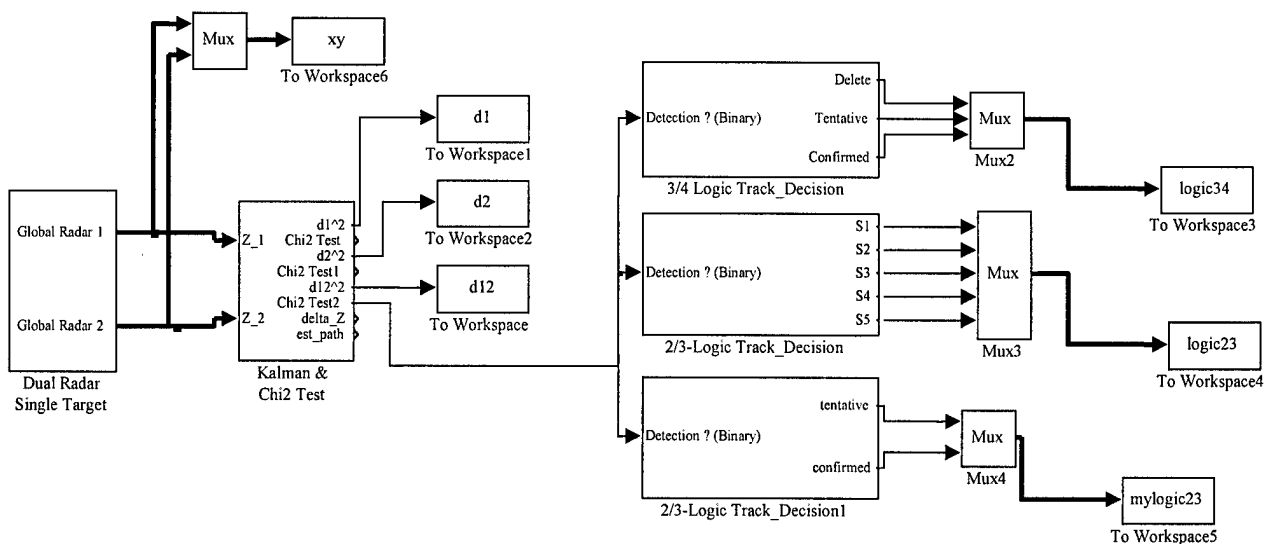


Figure 3-1 Top-Level Block Diagram

Figure 3-1 illustrates the top-level diagram of the simulation model. At the extreme left of the diagram is the target path generation and coordinate conversion block. This block passes the target paths from the two radars to the Kalman filter and Chi-square test block. The binary output of the Chi-square test is then passed to the track maintenance blocks which perform sequential testing to determine the track

state. The “to workspace” blocks collect test data which is then accessed from the MatLab[®] command line to implement Monte Carlo analysis.

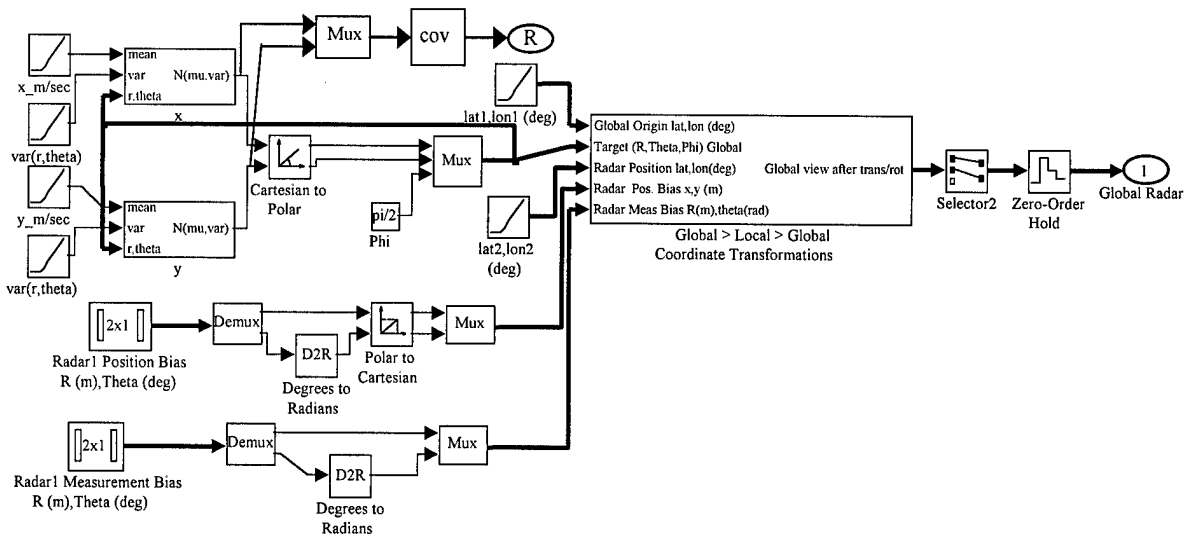


Figure 3-2 Path Generation Block Diagram

Figure 3-2 illustrates the block diagram responsible for generating the target path, measurement variances, position bias, range bias, and azimuth bias. The coordinate transformation block performs a global to local transformation, injects the biases, and then performs the local to global transformation for each radar. The relevant equations for the coordinate transformation are included in Appendix three.

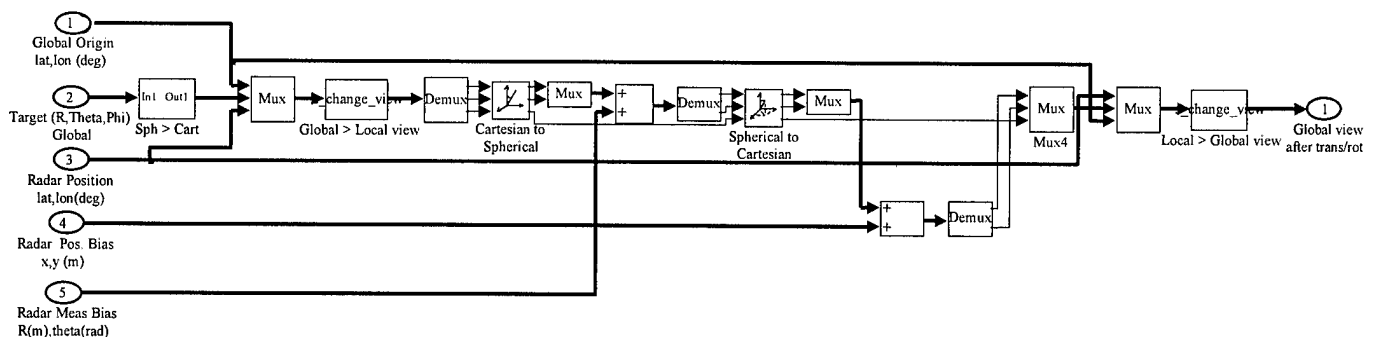


Figure 3-3 Coordinate Conversion and Bias Insertion Block Diagram

Figure 3-3 illustrates the internal block diagram responsible for local-to-global coordinate transformation, and the insertion of position, range and azimuth biases. Notice that the position biases are inserted in cartesian coordinate space, while the range and azimuth biases are inserted in spherical coordinate space. It may be intuitively obvious that the nature of these bias will influence the gate correlation process differently. More will be discussed about this topic in the analysis of results section of this paper.

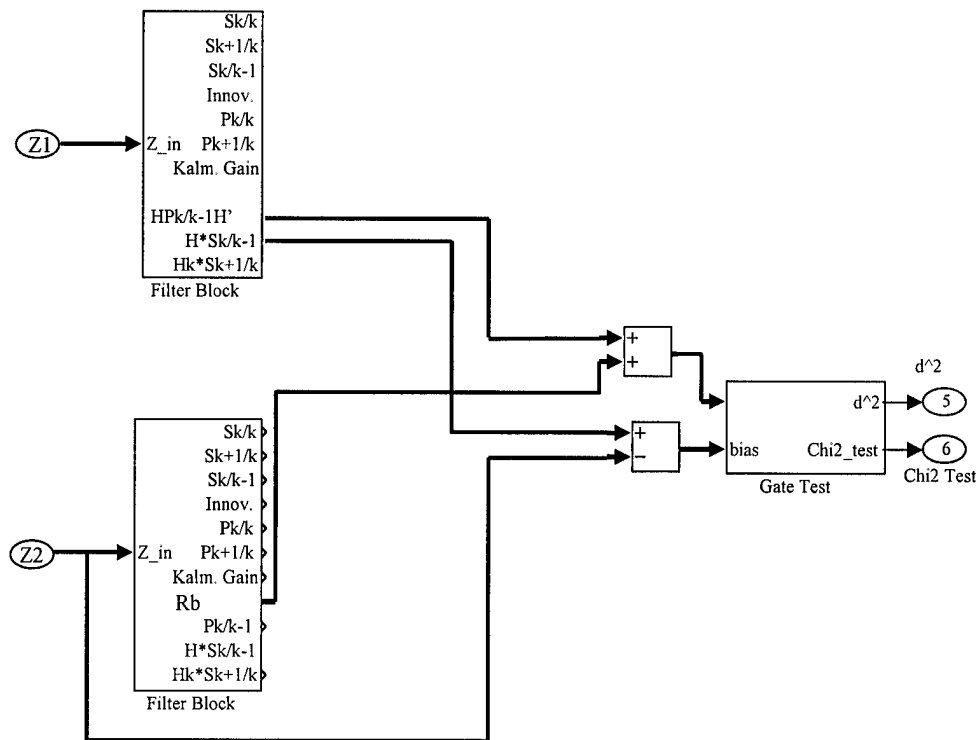


Figure 3-4 Kalman Filter and Chi-square Gate Test Block Diagram

Figure 3-4 illustrates the block diagram responsible for generating the target tracks and accompanying statistics which are passed to the Chi-square gate test blocks. Notice that the bias is simply the difference of the state position components from radar one and the measurements from radar two. The Kalman filters also pass the required measurement error covariance and state prediction error covariance required by the Chi-square gate test blocks.

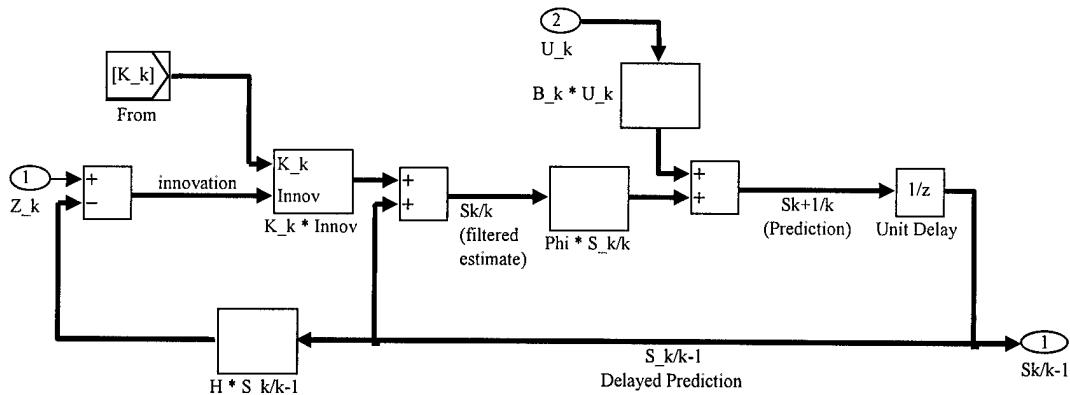


Figure 3-5 Kalman Filter State Estimation Loop

The Kalman filter consists of two distinct recursive “loops”. Figure 3-5 represents the Kalman filter state estimation loop which recursively estimates the current state and also calculates the one-step prediction of the next measurement. It can be seen that the prediction is delayed by the period between individual measurements which corresponds to the scan time for the mechanically rotated radar. The measurement components of the predicted state vector are extracted and then subtracted from the current measurement, resulting in the state estimation error commonly called the innovation or innovation process. The innovation is then “weighted” by the Kalman gain matrix (**K**), which is calculated in the Kalman filter covariance loop shown in Figure 3-6.

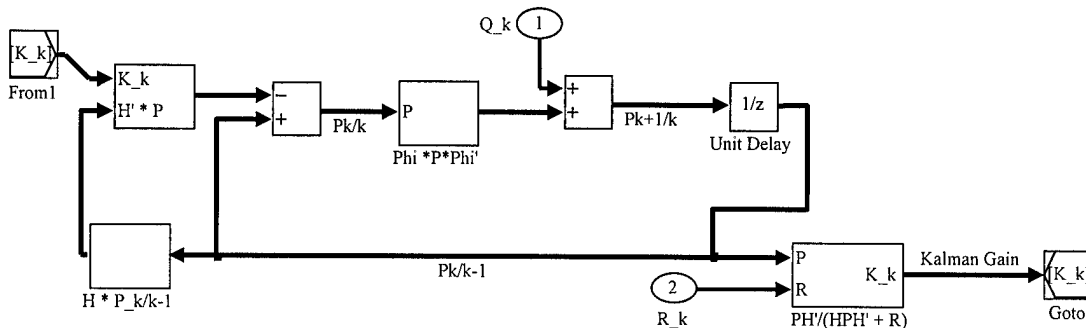


Figure 3-6 Kalman Filter Covariance and Kalman Gain Loop

As stated above, the Kalman gain is calculated in the covariance loop of the Kalman filter shown in Figure 3-6. It should be emphasized that the Kalman gain is independent of the state. This can be seen by noticing that the only inputs to the covariance loop are the process (or plant) error covariance (\mathbf{Q}), the measurement (or observation) error covariance (\mathbf{R}), and its previously calculated Kalman gain.

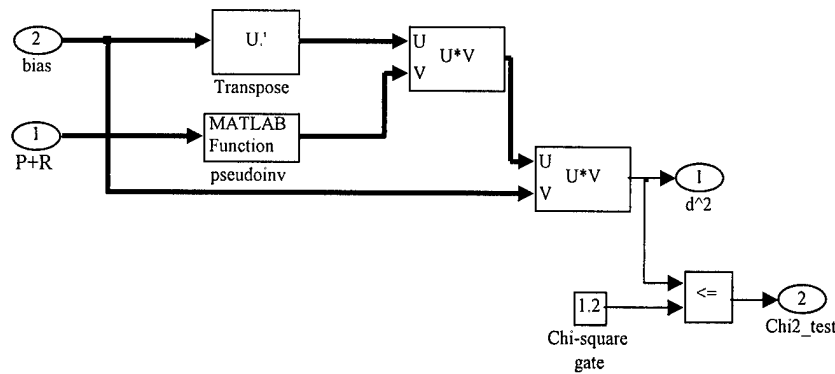


Figure 3-7 Chi-Square Gate Test Block Diagram

Figure 3-7 illustrates the internal block diagram of the chi-squared gate test block from Figure 3-4. This block performs the correlation criterion calculations described in equation (2.24) and compares this result to the gate size. Looking forward to the analysis of results section of this paper, the plots concerning the gating criterion correspond to d^2 in Figure 3-7. The MatLab[®] function that performs the inverse operation here is the pseudo-inverse function with an imposed tolerance of 10^{-6} . The pseudo-inverse function is used instead of the inverse or division functions due to the possibility of singularity of the innovation covariance matrix which may result from round-off errors.

The matrix multiplication blocks in Figure 3-7 require knowledge of the size of the matrices to be multiplied. These values cannot be changed during a simulation; this is the source of difficulty in passing varying sized matrices that would be required for representing missed measurements or extraneous clutter (false alarm) measurements. One may be able to define an initial arbitrarily large matrix capable of containing the maximum probable number of targets measured at any instant. In the event of a missed

target, the measurement value could be represented by not a number (NaN). The algorithms that operate on the measurements would then need to be capable of detecting the NaN and either suspend calculation, or hold the previous calculated value.

3.3 Assumptions

A number of assumptions are asserted in order to simplify the creation of the simulation model. These assumptions may be grouped into the following topics:

3.3.1 Fixed Sample (or Measurement) Intervals

Although a fixed measurement interval is assumed, an actual rotating radar antenna generally will not measure a moving target at a fixed interval unless the target path is strictly radial. This assumption is made primarily due to the difficulty of implementing varying sample times in Simulink®. It should be noted however, the Kalman filter algorithm doesn't required fixed sample intervals, thus future amendments to this model may remove this assumption.

3.3.2 Single Target

A single target is assumed in this analysis. This is done since, as eluded to earlier, each target requires a dedicated Kalman filter. Additionally, the influences of biases in the single target case will also apply for multiple targets assuming that dedicated Kalman filters are required for each target. This assumption does however, exclude the analysis of situations such as crossing targets, and closely separated targets (formations).

3.3.3 No Clutter / False Alarms

The assumption that no false alarms occur is made for reasons similar to the single target argument. In the event that clutter generates false alarms, a bank of Kalman filters is needed to process all potential tracks since it cannot be determined if the detection is due to clutter or a real target. Future

amendments to this model would gain from the vectorization of the Kalman filter algorithm. This may be accomplished by implementing an S-function capable of processing varying width vectors.

3.3.4 100 % Probability of Detection

It is assumed that each target is detected once on each scan. While this assumption rarely reflects reality, the difficulty of processing missed detections necessitated its acceptance. A missed detection must be represented mathematically in the simulation model. At each observation, the Kalman filter accepts the target's spatial coordinates and performs the ensuing calculations. Representing the missed detection as a vector of 0s impacts the calculation of the predicted state to varying degrees, depending on the previous measurement and state. To remove this assumption, some method must be used to alleviate this problem.

4. Analysis of Results

4.1 Overview

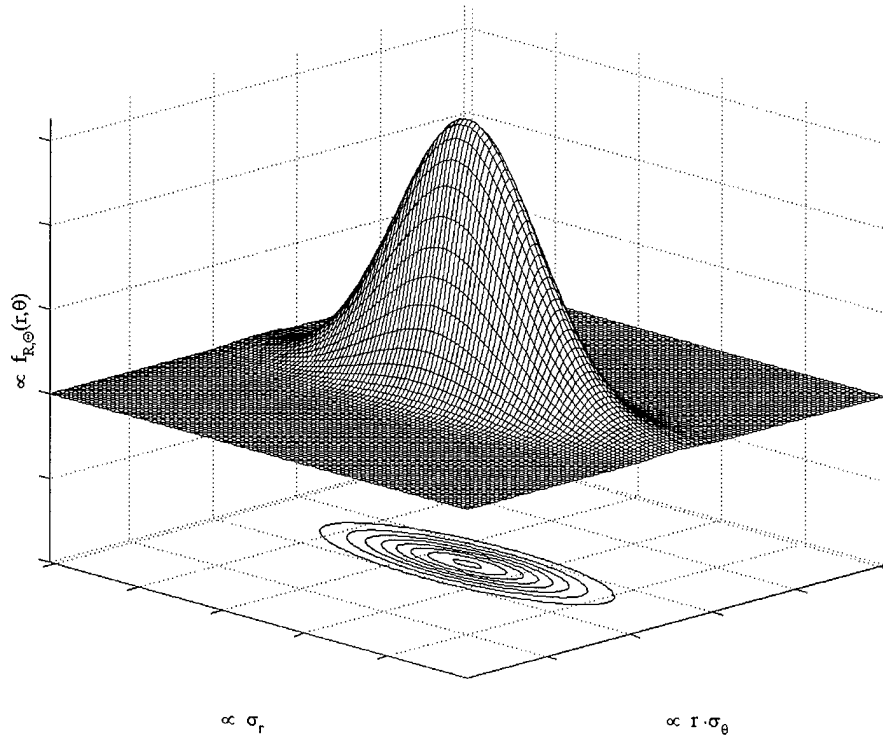


Figure 4-1 Representative Constant-Error Ellipses

Refer to Figures 4-1 and 4-2 to help visualize the following discussion. A substantial portion of current literature assumes that the cross-range semi-axis ($r \cdot \sigma_\theta$) is much greater than the down-range semi-axis (σ_r) when analyzing worst case radar-target geometries[Bar90]. In an effort to model a realistic networked surveillance radar system, the following measurement statistics are chosen: $\sigma_\theta = 0.18$ degrees ($\text{deg} \cong \pi \cdot 10^{-3}$ radians (rads) and $\sigma_r = 0.125$ nautical miles (nmi) $\cong 231.5$ meters (m)[Bar90]. Recalling that the semi-axes of the constant-error ellipses are equal to σ_r and $r \cdot \sigma_\theta$, and considering the self-imposed maximum detectable range of approximately 100 Km, this corresponds to $r \cdot \sigma_\theta \cong 100,000 \text{ m} \cdot \pi \cdot 10^{-3} \text{ rads} \cong$

314 m. Due to the target path geometries chosen, the minimum down-range distance is nearly 35,000 m, resulting in $r \cdot \sigma_\theta \cong 35,000 \text{ m} \cdot \pi \cdot 10^{-3} \text{ rads} \cong 109 \text{ m}$.

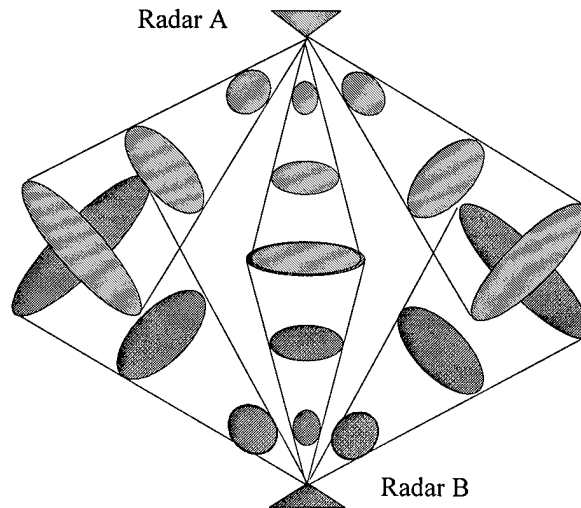


Figure 4-2 Constant-Error Ellipses vs. Target Position

The down-range measurement variance is not a function of range but of the specific parameters of the radar such as pulse width, number of pulses integrated, Doppler frequency, clock stability, etc. Because of this fact, the range independent $\sigma_r \cong 231.5 \text{ m}$. The range at which the measurement error ellipse becomes circular is $r = \sigma_r / \sigma_\theta \cong 231.5 / (\pi \cdot 10^{-3}) \cong 73,688 \text{ m}$.

Having determined the constant-error ellipse dimensions, it is observed that the ellipses will not be highly eccentric, but rather oval or circular contours. Furthermore, the area (A) of the constant-error ellipses can be calculated by $A = \pi \cdot r \cdot \sigma_\theta \cdot \sigma_r$. It is obvious that the maximum area (A_{\max}) will occur at the maximum detectable range, $A_{\max} \cong \pi \cdot 100,000 \text{ m} \cdot \pi \cdot 10^{-3} \text{ rads} \cdot 231.5 \text{ m} \cong 228,481 \text{ m}^2$. Likewise, the minimum area (A_{\min}) will occur at a down-range distance of 35,000 m, then $A_{\min} \cong \pi \cdot 35,000 \text{ m} \cdot \pi \cdot 10^{-3} \text{ rads} \cdot 231.5 \text{ m} \cong 80,000 \text{ m}^2$.

All of the following simulations are performed thirty times for each increment of the independent variable, the minimum required to assert the Gaussian assumption in the confidence level

calculations. The initial seed for each random number generator is uniquely determined for each run as a function of the system clock.

4.2 Positional Bias

Radars A and B are positioned at (50 Km, 100 Km) and (50 Km, 0 Km) in global Cartesian coordinates, respectively, and the global origin is at (0, 0), as shown in Figure 4-3. The target travels in a diagonal path at 200 m/sec in the -x and -y directions. The initial detection of the target is at (100 Km, 100 Km) in global Cartesian coordinates. Thus the target is centered between radars A and B after 250

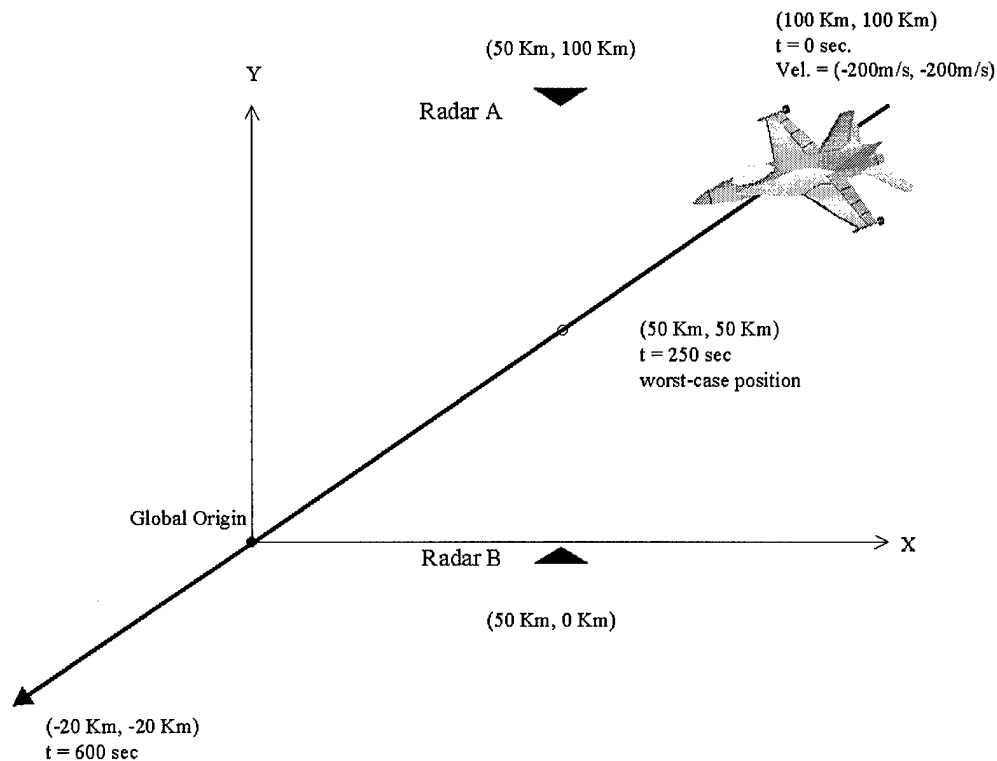


Figure 4-3 Position Bias Target Path

seconds have elapsed after initial detection. The injected biases at either of the radars A or B are such that they are directed along the x-axis. The measurement error ellipses at this point are greater in the down-range direction than they are in the cross-range direction. In the absence of the cross-range biases,

these ellipses “line-up”, however due to the biases, they are misaligned by relative value of the bias between radars A and B.

When calculating the upper bound on the position bias, the minimum detected range is about 35 Km, however the range occurring during the worst-case geometry is 50 Km. If the smaller down-range distance is used, $|\mathbf{b}_p| = 1.34 \cdot 35 \text{ Km} \cdot \pi \cdot 10^{-3} \cong 147 \text{ m}$. Alternatively using the worst-case range of 50 Km, $|\mathbf{b}_p| = 1.34 \cdot 50 \text{ Km} \cdot \pi \cdot 10^{-3} \cong 210 \text{ m}$. As illustrated in Figure 4-4, the simulated $|\mathbf{b}_p| \cong 180 \text{ m}$ falls approximately at the midpoint of these two values.

Since these positional biases cause the same misalignment everywhere in the detectable area, the worst-case geometry is determined merely by the eccentricity of the ellipses and the orientation of the ellipses with respect to the biases.

It can be seen in Figure 4-4 that, as predicted by our previous development of Chapter two, the worst-case radar-target geometry occurs when the target is centered between the two radars and the positional bias is perpendicular to the line joining the two radars. It should be noted that position biases do not generate as pronounced effects in the worst-case geometry as do the range and azimuth biases, as will be shown. Lambda, the variable along the vertical axis in Figure 4-4, represents the total normalized bias, or equivalently, the noncentrality parameter in the Chi-square distribution.

The transient properties of the Kalman filter cause the small initial Chi-square test results. This occurs because the initial confidence in the measurements is small, so the measurements (and added position bias) are weighed less heavily. In this case, the filter relies more upon its predicted measurement which is derived from the filter’s linear target path model. It should be noted here that the simulation results depend to some extent on the initial values of the prediction error covariance matrix, P_0 , and the initial state values, S_0 . The a priori knowledge of the initial target location and velocity allows determines the S_0 , and the process and measurement statistics determine P_0 .

Figure 4-5 is the one-sided confidence level from the position bias simulation, and is included for completeness.

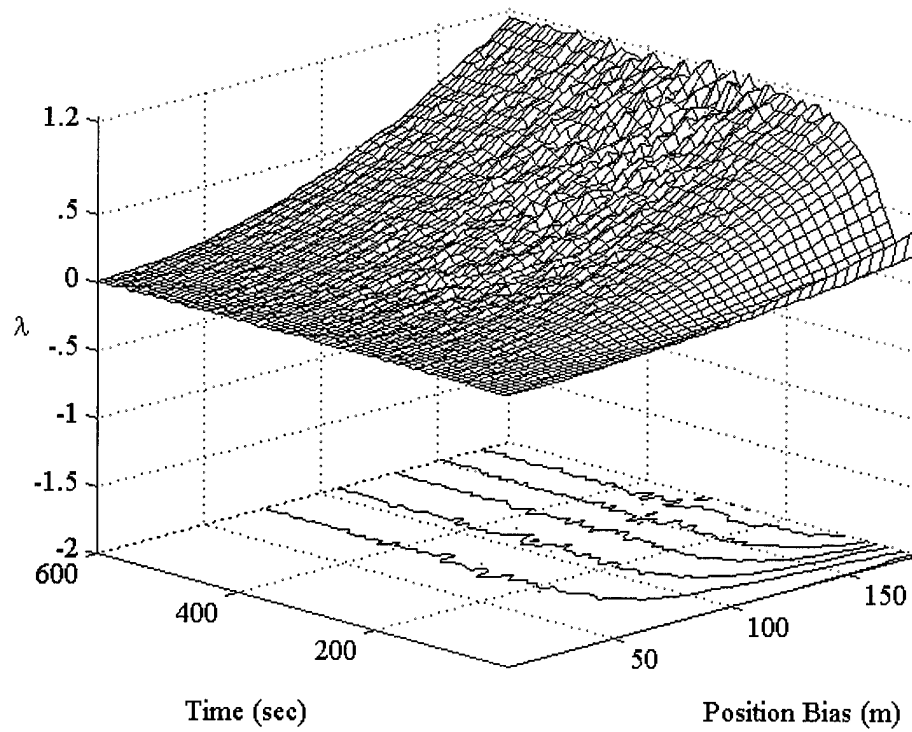


Figure 4-4 Position Bias vs. Target Position

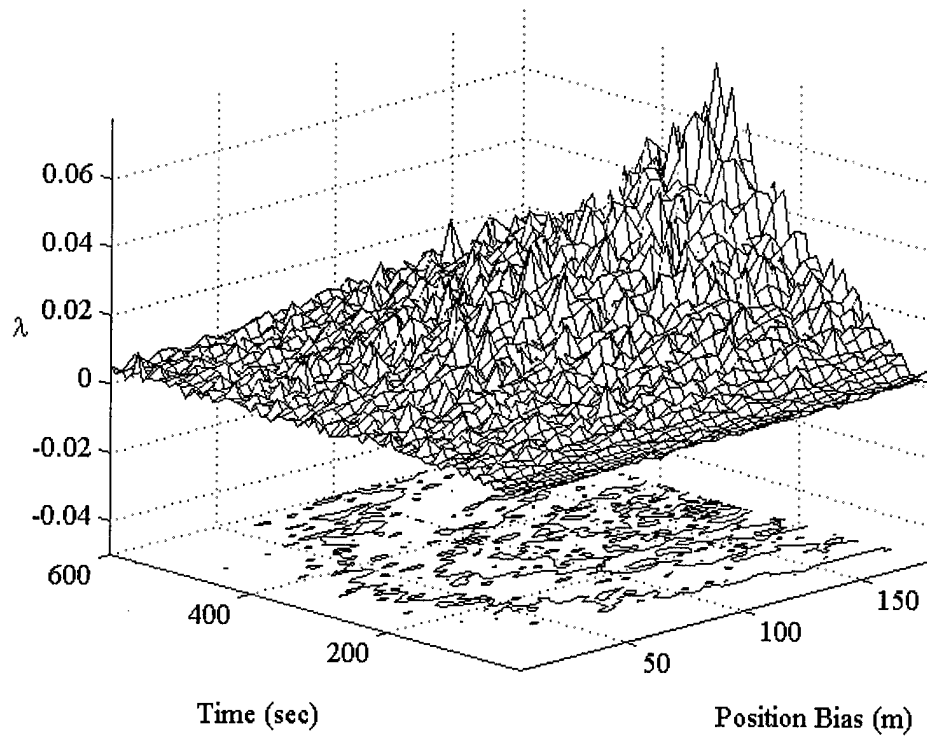


Figure 4-5 Position Bias 95% Confidence Level (one-sided) vs. Target Position

4.3 Range Bias

Figure 4-6 illustrates the radar-target geometry chosen for the range bias simulation. This geometry is chosen to minimize the initial convergence effects of the filter, and to allow the target path to pass through the (50 Km, 50 Km) position to observe the effects of an orthogonal radar-target geometry.

As with the positional biases, the worst-case geometry for range biases occurs for a target centered between the two radars. The biases in this case however, are down range biases of equal value resulting in a misalignment of the measurement error ellipses in varying directions depending on target position. The theoretical range bias required at each radar to yield the non-centrality parameter $\lambda = 1.2$ is, $|\mathbf{b}_r| = 0.67 \cdot \sigma_r \cong 155$ m. Figure 4-7 illustrates the simulated bias value necessary to reach the non-centrality value is somewhat higher, nearly 180 m. This may be explained by the fact that the range bias shifts the error ellipses along their major semi-axes since the down-range variance is greater than the cross-range

error in this position. Meanwhile, the theoretical bound on the range bias assumes the cross-range error is much greater than the down-range variance. At the worst-case position, $\sigma_r \cong 231.5$ m, while $r \cdot \sigma_\theta = 35$ Km $\cdot \pi \cdot 10^{-3} \cong 110$ m.

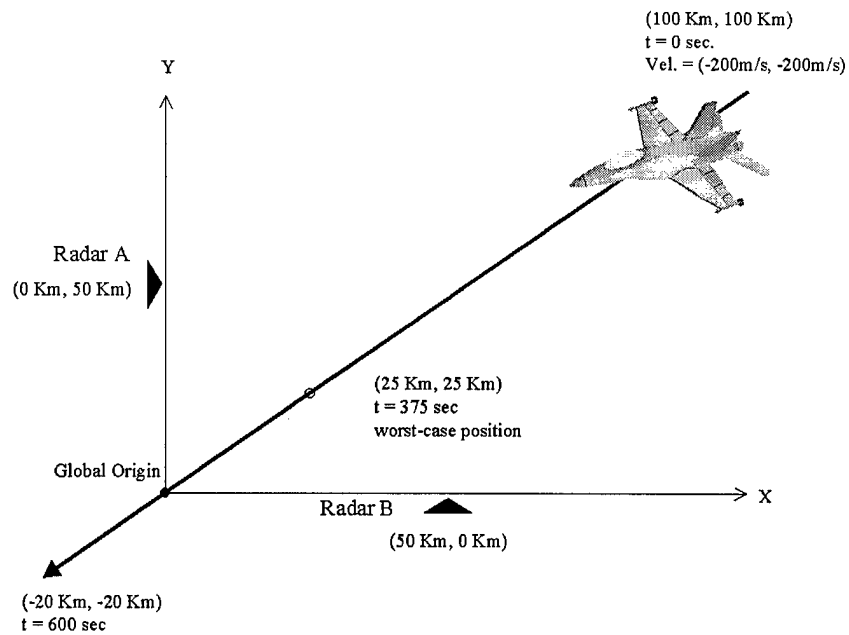


Figure 4-6 Range Bias Target Path

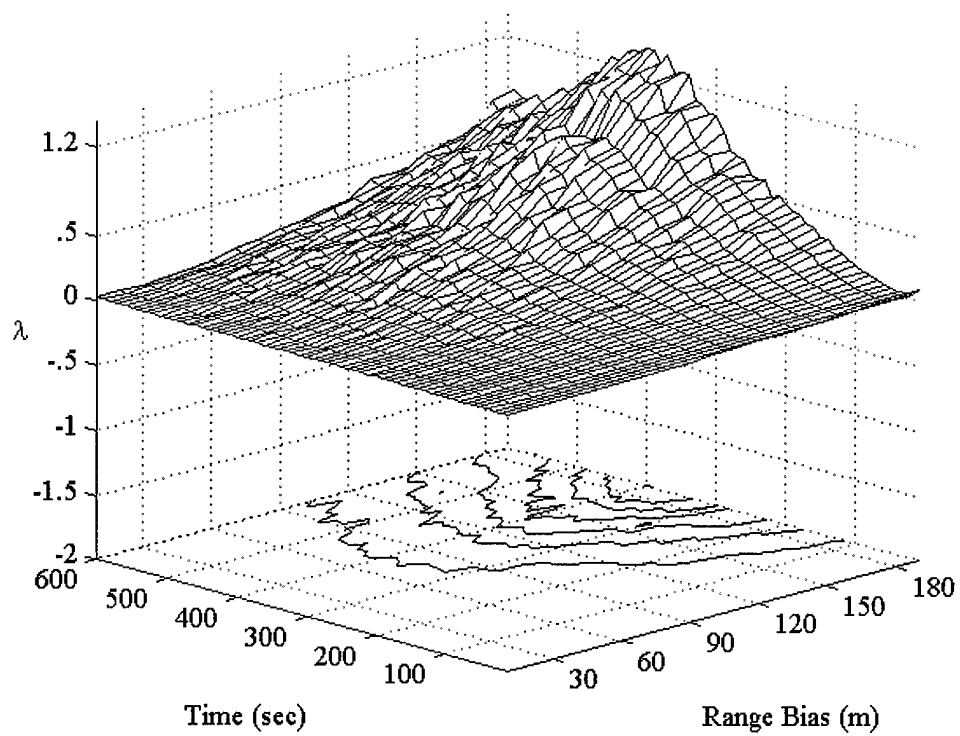


Figure 4-7 Range Bias vs. Target Position

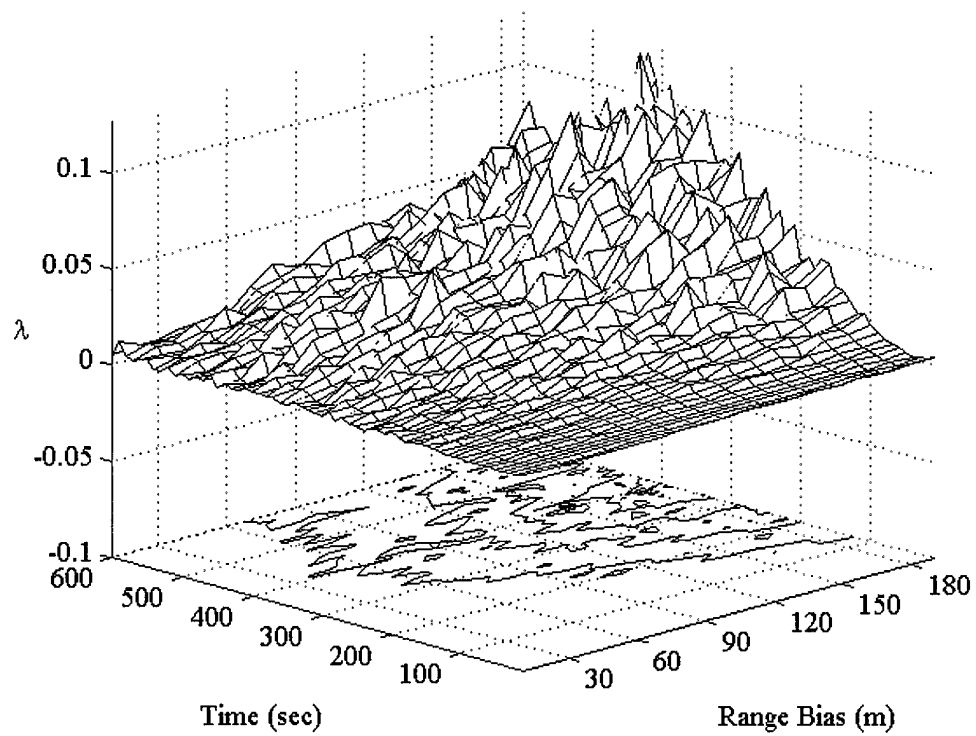


Figure 4-8 95% Confidence Level Range bias vs. Target Position

4.4 Azimuth Bias

For the analysis of the azimuth bias effects, the radar-target geometry illustrated in Figure 4-3 is again chosen to place the worst-case target position near the center of the path. As discussed in Chapter two, since the down-range variance is greater than the cross-range variance, the worst-case case radar-target geometry occurs at the midpoint of the line joining the two radars. The effect of the azimuth biases at this worst-case position is similar to the effect of position bias, since the measurement will be shifted, if not along the x-axis, at least tangential to the x-axis. The bound for the allowable azimuth bias is then calculated as $|\mathbf{b}_\theta| = 0.67 \cdot \sigma_\theta \cong 0.67 \cdot 0.18 \text{ deg} \cong 0.12 \text{ deg}$.

Figure 4-9 reveals the azimuth bound to be approximately 0.11 deg, which seems reasonable in light of Figure 4-10 which shows that the one-sided 95% confidence interval is nearly 0.1λ .

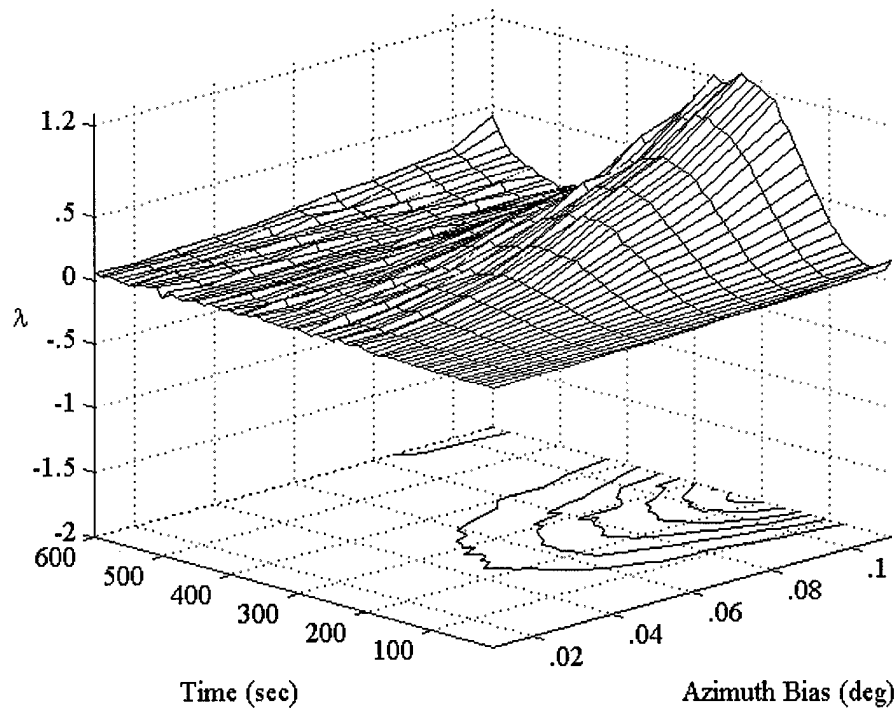


Figure 4-9 Azimuth Bias vs. Target Position

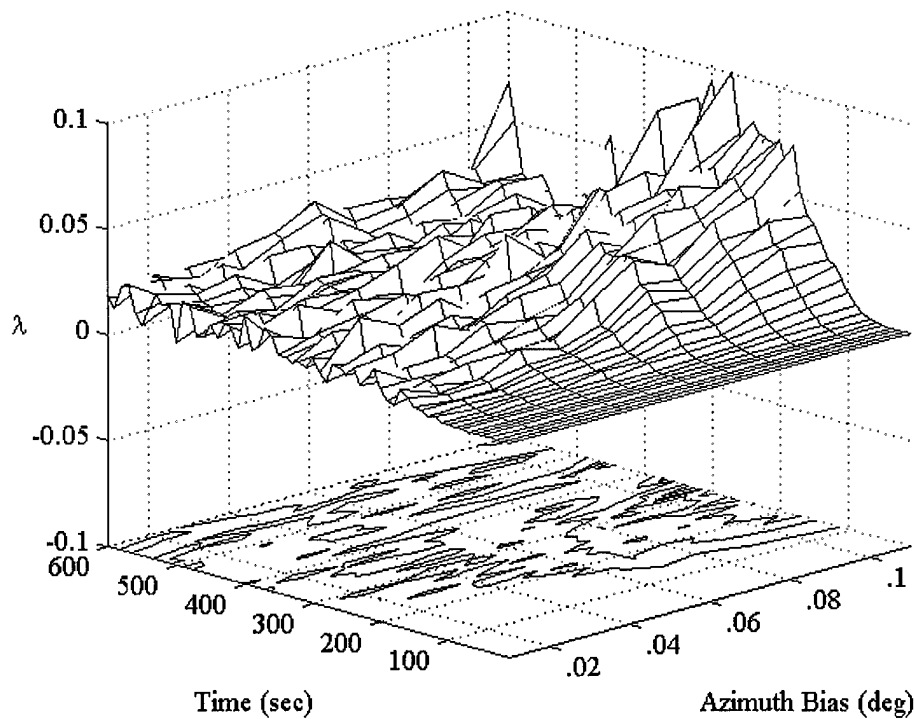


Figure 4-10 95% Confidence Level of Azimuth Bias vs. Target Position

4.5 Simultaneous Position-Range-Azimuth Biases

Finally, the radar-target geometry shown in Figure 4-6 is chosen for the simultaneous position, range, and azimuth bias simulation such that the influence of an orthogonal radar-target geometry may be examined, if they exist. The worst-case radar-target geometry for all three types of biases happens to occur at the same position, namely at the midpoint of the line joining the two radars. Recall that the position bias is a relative bias, effectively shifting the measurements an equal amount regardless the position of the target. Contrary to the position bias, the range and azimuth biases affect the measurements differently depending on the target's position relative to the radar.

Since the azimuth bias seems to have the most position-dependent properties, the simultaneous effect of the three biases is analyzed by setting the position and range biases at their upper bound, then assign the azimuth bias as the independent variable.

That is $|\mathbf{b}_p| = 0.77 \cdot r \cdot \sigma_\theta \cong 0.77 \cdot 35 \text{ Km} \cdot \pi \cdot 10^{-3} \cong 85 \text{ m}$, since the worst-case position coincides with the minimum detectable range for this flightpath. The range bias is calculated as $|\mathbf{b}_r| = 0.39 \cdot \sigma_r = 0.39 \cdot 231.5 \text{ m} \cong 90 \text{ m}$. The upper limit on the azimuth bias is calculated as $|\mathbf{b}_\theta| = 0.39 \cdot \sigma_\theta = 0.39 \cdot 0.18 \text{ deg} \cong 0.07 \text{ deg}$.

The results of the simultaneous position, range, and azimuth simulation illustrated in Figure 4-11, compares favorably with the theoretical simultaneous upper bounds on each of the biases in consideration of the one-sided confidence interval of Figure 4-12. The simulated azimuth bias required to exceed the upper bound on the correlation criterion is $|\mathbf{b}_\theta| \cong 0.06 \text{ deg}$. It may be observed that the result of combining these biases tends to “blend” the spatial properties of each, that is the relatively position-independent property of the position bias and the more position-dependent properties of the range and azimuth combine to form a moderately position-dependent response. Of course the convergence of the Kalman filter’s covariance matrix causes the “slow” transient response immediately after initial detection.

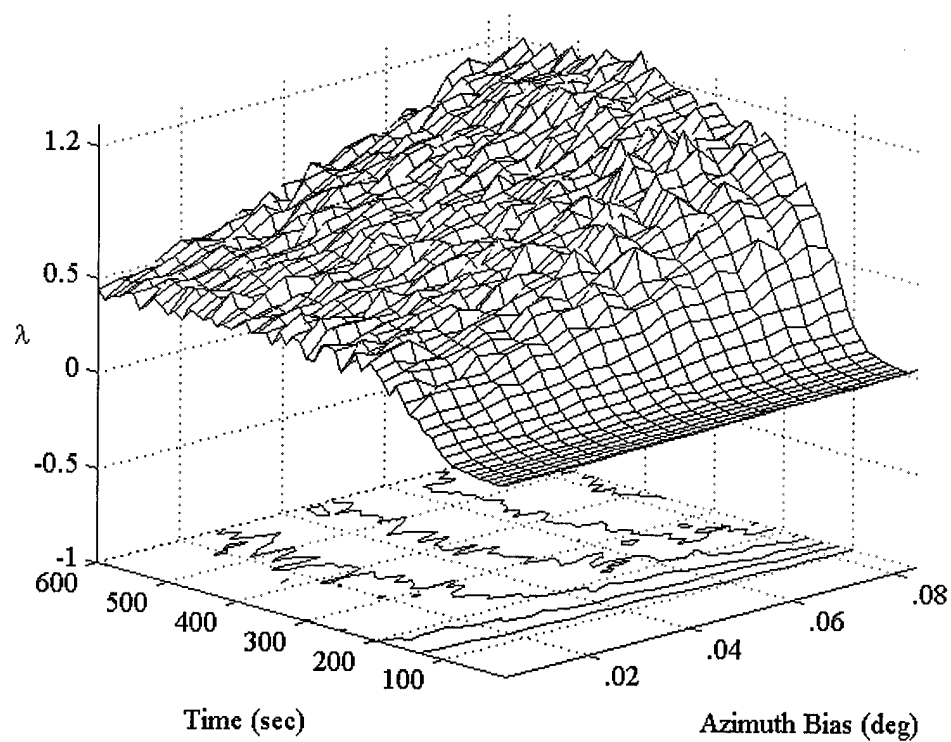


Figure 4-11 Simultaneous Position-Range-Azimuth Bias vs. Target Position

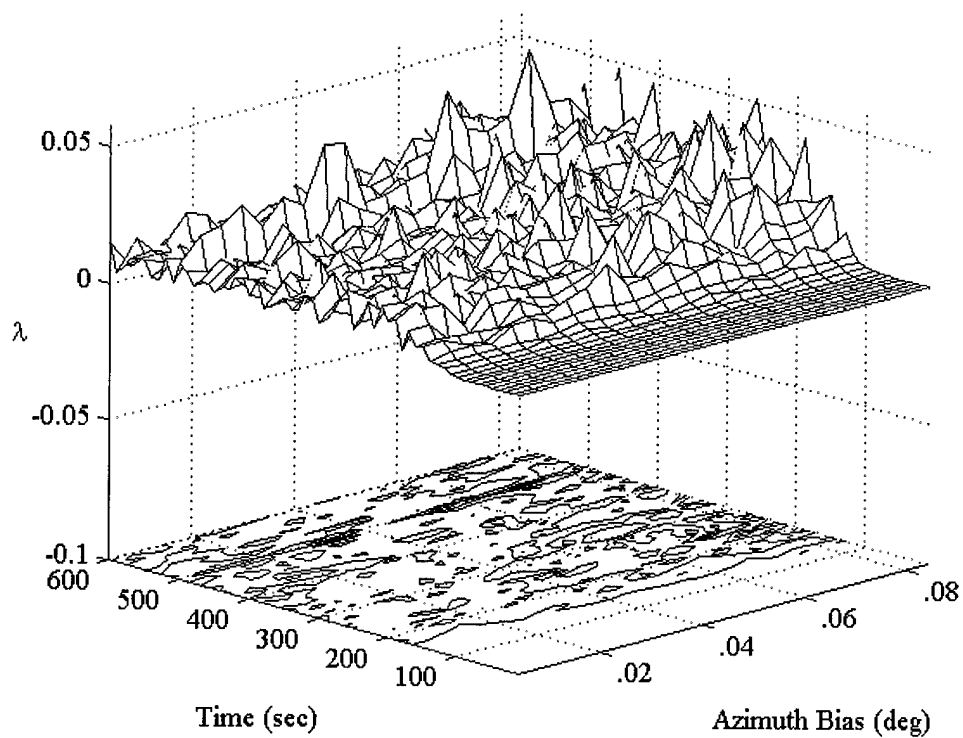


Figure 4-12 Position-Range-Azimuth 95% Confidence Level

5. Summary / Recommendations

This thesis examines the effect of registration errors, namely, position, range, and azimuth biases both individually and collectively. The worst-case radar-target geometries may be predicted given knowledge of the down-range and cross-range measurement error statistics. The quantitative effects of the biases may be analyzed by employing statistical correlation gates. These elliptical correlation gates are defined by the Chi-square statistics of the measurement errors. The degree of ellipticity of these equal-probability contours are governed by the measurement error statistics and the down-range distance.

5.1 Coordinate Transformations

To gain an advantage from measurements at multiple distributed radars, the measurements must be transformed into a common reference frame. To remove the inherent weakness of two-dimensional radar to determine correct slant range, target returns are generated in three dimensions. The individual radar measurements are then transformed into “global” coordinates. First the radar geographical coordinates are transformed to geocentric coordinates using an ellipsoid to approximate true earth geoid shape. The local coordinate system of one radar is then transformed to that of another, or alternatively to an arbitrary “global” coordinate system through a translation and a series of rotations, (see Appendix 3).

5.2 Kalman Algorithm

Presented in Appendices 1 and 2 is the development of the discrete Kalman filter difference equations which provide the minimum variance, or most accurate estimate of the actual target position. The Kalman filter employs an embedded model of the system, which in this case is a target traversing a linear path in cartesian coordinates. The Kalman filter is a recursive estimator, with the advantage that the required memory, or sample length, does not increase with time. All the needed information is stored in the state and error covariance matrices.

Two approaches to the development of the Kalman filter equations are provided. The first assumes that the noise processes and the initial state are normally distributed, and the mean-square estimate criterion is then used to obtain an optimum filter which estimates the state conditioned on the measurement. From the assumptions of a linear model and Gaussian statistics, a linear filter results.

The second approach is the linear mean-square estimator, which makes no assumptions about the process distribution functions. This approach makes use of the orthogonality between the estimation error and the observations, the concept of the innovation sequence, and a recursive updating formula for the estimate when a new measurement is available.

5.3 Analytical Model Development

Given that the radar measurements are independent Gaussian distributed random variables, the mean-square error criterion is a Chi-square distributed random variable, i.e., the sum of squared independent Gaussian random variables is a Chi-square distributed random variable. The maximum allowable bias is determined by choosing a minimum probability of correlation between two radar measurements based on the desired system track accuracy. Each imposed bias is then viewed as the non-centrality parameter of a non-central Chi-square distributed random variable, which allows for the determination of whether or not the two measurements “probably” come from the same target. Given this metric, the allowed biases in position, range, and azimuth may be quantitatively determined.

5.4 System Model

Given that tracking is performed for a target with a linear path (underlying assumption), the appropriate state transition matrix is a linear function of the previous position and the product of target velocity and observation interval. The radars measure only position, however, to make a more accurate prediction the state vector is augmented to include velocities in the x and y directions. The observation matrix, therefore, merely extracts the position components of the state vector.

Due to the linearity of the system, the next state is determined by the superposition of the effect of the actual state value and the effect of the input noise. The state-transition matrix accounts for the contribution to the predicted state of the past history of the system “stored” in the present state. The observations are linear combinations of the state components, which are corrupted by additive noise.

5.5 Bias Effects

As predicted by the analytical model, position bias is relative. That is, if both radars have the same vector bias, their measurements fall within the correlation gate most of the time, no matter how large the bias. Thus for the worst-case bias, antipodal biases are imposed, i.e., opposing vector biases, for each of the two radars. Notice that the position biases impose a relatively constant correlation criterion regardless of the relative radar-target geometries. The nature of the constant-error contours determines the worst-case radar-target geometries and the vector direction of the worst-case biases. The range variance is larger than the cross-range variance for the chosen measurement statistics and radar coverage area. Thus, worst-case positional bias occurs when the target is centered between radars and the bias is perpendicular to the imaginary line joining the two radars.

The worst-case geometry for range biases is the same as for position biases, however, range biases are not relative, and each radar can contribute an error. Whether these errors are additive or partially cancel each other depends on the exact geometry and on the sign of the bias, which explains why range bias shows more position dependence than does position bias.

The worst-case geometry for the azimuth biases coincides with the position and range worst-case geometries. The azimuth biases are also more position dependent than the position biases. In the imposed radar-target geometry, the cross-range variance is minimum when the target is at the mid-point of the line connecting the two radars. Thus, the worst-case bias scenario is for both radars to have azimuth biases in the same rotational direction.

Combining all three biases simultaneously results in a more position dependent response. Of course in the general case the effect of simultaneous position, range, and azimuth biases varies depending upon radar measurement statistics, down-range distance, radar-target geometries, and the relative vector directions of the biases.

5.6 Recommendations

The implemented model allows for the simulation of one target tracked by two spatially distributed radars, yet much may be done to improve the usefulness of this model. The following paragraphs present a number of recommendations and discusses their possible implementation.

5.6.1 Vectorize the Kalman filter algorithm

To process all incoming signals from the radar detection hardware, not one Kalman filter but an entire bank of filters must be used to formulate the statistics for all potential targets, whether they are from actual targets or from false clutter detections. Some functions in MatLab[®] accept variable vector “widths” as input. It would be advantageous to “vectorize” a Kalman algorithm function so that at each discrete moment any detection within the radar range-azimuth detection gate could be processed as a confirmed track, a tentative track, or a new detection.

The vectorization may be realized by representing the Kalman filter difference equations in their z-transform transfer function form. The inclusion of the initial state values would be necessary for this method to correctly represent the Kalman filter algorithm. Additionally, the measurement statistics must be observable at each instant to allow execution of the Chi-square gate test.

5.6.2 Accept ASCII/MAT plot files

As stated earlier, output plot (or detection) files from accepted radar simulation software packages should be acceptable input to the simulation model. In MatLab[®], .mat files are ASCII text files

formatted such that the monotonic increasing or decreasing independent variable is in the first row of the file and the accompanying dependent variables are in the remaining rows. In the event that the input is already in this format, integration is easily executed with the load command. However, if the data provided is in another format, the primary difficulty is converting the file to .mat format.

5.6.3 *Multiple Radars*

In the event that more than two radars detect a target within the same correlation gate in a networked radar system, the measurement statistics from all radars may be processed together to take full advantage of sensor fusion. This joint processing could be performed by a series of cascaded Kalman filters, in which the first stage is a bank of Kalman filters and each filter processes, (fuses), all possible combinations of detected targets in a correlation gate. The number of filters required in the ensuing levels of the cascade would of course decrease by a factor of two. Alternatively, after the first level of the cascade the statistical distances may be compared to select the smallest distance so that the track may be updated with a filtered estimate.

5.6.4 *Degradation of Tracking Accuracy*

This thesis addresses the worst case situation in a networked radar system, i.e., the case where biases force the initiation of additional tracks for a single target. As discussed in the introduction, biases may introduce a continuum of tracking degradation effects, from reduced accuracy relative to maximum theoretical accuracy to the creation of a separate track. To actually estimate the biases of each radar and correct for them is a much more difficult problem. It may be shown that the ability to accurately estimate these biases is proportional to the number of available targets in overlapping coverage areas and the radar-target geometries[Bar90].

The Munkres algorithm mentioned earlier, provides the optimum assignment in the event of N tracks and M detections, (where there may be more or less tracks than detections). The Munkres

algorithm is essentially a recursive matrix reduction algorithm which performs subtraction in row or column space while continually testing for the “closest” detection for each track[Bla86]. Although the results reported here do not use the Munkres algorithm, MatLab[®] code implementing this algorithm is included in Appendix 4.

5.6.5 *The Effect of Sample Time*

It may be informative to investigate the behavior of error covariances when the observation interval becomes longer. More precisely, it may be worth determining whether finite limit values exist for the error covariances as the observation interval becomes large and under what conditions they are independent of the initial value of the error covariance.

5.6.6 *Multiple-Hypothesis Tracking*

Although a constant velocity target is assumed here, many situations may occur where the target maneuvers significantly for a period of time. In this case the assumed linear system model is no longer valid, instead a constant acceleration model may be implemented when the target no longer falls within the correlation gate. When, (or if), the target resumes a constant velocity profile, the assumed model may revert back to the linear model. In essence then, it can be assumed or hypothesized that the target path has multiple “modes” or profiles, hence the name multiple-hypothesis tracking. Of course multiple modes are more difficult to implement than the single system model, and problems linked to this switching process must be solved to maintain tracking continuity between multiple system models.

1A. Appendix 1 Kalman Filtering Introduction

1A.1 Linear System Model

In many estimation problems, an unknown vector represents the time evolution of a system, and the measurements \mathbf{Z} are the observed output from the system. The state-variable approach is a valuable method to describe such dynamic systems where the input-output relationship is described in the time domain by a state-transition model together with an output observation model. The state represents the internal condition of the system and accounts for its memory of past inputs. The inputs may consist of deterministic functions of time together with stochastic processes representing unpredictable variables or noise. The output is a function of the state, usually corrupted by random measurement errors.

A discrete-time system is described by the following pair of equations:

$$\mathbf{S}_{k+1} = \mathbf{F}(\mathbf{S}_k, \mathbf{U}_k, \mathbf{V}_k, k) \quad (1A.1)$$

$$\mathbf{Z}_{k+1} = \mathbf{G}(\mathbf{S}_{k+1}, \mathbf{W}_{k+1}, k+1) \quad (1A.2)$$

Where the integer subscripts $(k, k+1)$ denote discrete-time instants,

\mathbf{S}_k is an n -dimensional vector representing the state at time k ,

\mathbf{U}_k is a p -dimensional vector representing the deterministic control inputs,

\mathbf{V}_k is the q -dimensional random vector representing the model process (or plant) noise,

\mathbf{W}_k is an r -dimensional random vector representing the observation (or measurement) noise, and

\mathbf{Z}_k is the m -dimensional vector of the observations (or measurements).

$F(\cdot)$ accounts for the state transition from S_k to S_{k+1} due to the input (U_k, V_k) occurring at time k . $G(\cdot)$ performs the projection of the internal state on the output measurable variables Z_{k+1} , as well as the effect of the random errors W_{k+1} . The explicit dependence on k accounts for a possibly non-stationary system.

A fundamental case to be considered is that of linear systems, primarily because of their practical interest and also because complete results in estimation theory are available for this class of systems.

Equations (1A.1) and (1A.2) particularize to the following:

$$S_{k+1} = \Phi_k S_k + B_k U_k + G_k V_k \quad (1A.3)$$

$$Z_{k+1} = H_{k+1} S_{k+1} + L_{k+1} W_{k+1} \quad (1A.4)$$

where $\Phi_k, B_k, G_k, H_{k+1}, L_{k+1}$ are real-valued matrices having dimensions $(n \times n), (n \times p), (n \times q), (m \times n), (m \times r)$, respectively. Equation (1A.3) shows that, because of the linearity of the system, the next state S_{k+1} is determined by the superposition of two terms: the effect of the actual state value S_k and that of the input samples U_k and V_k . The state-transition matrix Φ_k , accounts for the contribution to S_{k+1} of the past history of the system, stored in S_k . In particular, when input-free conditions occur (i.e. $U_k = 0$ and $V_k = 0$), the state depends on the initial condition S_0 only, according to the equation

$$S_{k+1} = \Phi_k \cdot \Phi_{k-1} \cdot \dots \cdot \Phi_1 \cdot \Phi_0 \cdot S_0 \quad (1A.5)$$

In this case, the stability of the system, i.e. the condition for S_k to remain bounded, depends on the matrices Φ_j ($j = 0, 1, \dots, k$). The matrices B_k and G_k account for the possibility of the system being forced into a new state by input variables. Equation (1A.4) shows that the observations Z_{k+1} are linear combinations of the state components, corrupted by additive noise. The matrix H_{k+1} indicates how the components of S_{k+1} are combined to form the observed vector S_{k+1} and therefore accounts for the ability of the system state to be determined from the measurements.

In order to complete the description of discrete-time linear systems, it is worth deriving the time evolution of the statistics of \mathbf{S}_k and \mathbf{Z}_k when a random input \mathbf{V}_k is present. Let \mathbf{V}_k and \mathbf{W}_k be zero-mean, white processes having the following covariance matrices:

$$E\{\mathbf{V}_j \mathbf{V}_k^T\} = \mathbf{Q}_k \delta_{kj} \quad (1A.6)$$

$$E\{\mathbf{W}_j \mathbf{W}_k^T\} = \mathbf{R}_k \delta_{kj} \quad (1A.7)$$

$$E\{\mathbf{V}_j \mathbf{W}_k^T\} = \mathbf{0} \quad (1A.8)$$

where δ_{kj} is the Kroenecker operator ($\delta_{kj} = 0$ if $k \neq j$ and $\delta_{kk} = 1$) while \mathbf{Q}_k and \mathbf{R}_k are positive semi-definite real matrices. These matrices describe the correlation between the different components of \mathbf{V}_k and \mathbf{W}_k , at the same time sample k , whereas no correlation exists between samples taken at different times (white processes). The expected value of \mathbf{S}_k is simply obtained from equation (1A.3) as

$$E\{\mathbf{S}_{k+1}\} = \Phi_k \cdot E\{\mathbf{S}_k\} + \mathbf{B}_k \cdot \mathbf{U}_k \quad (1A.9)$$

And similarly for \mathbf{Z}_k ,

$$E\{\mathbf{Z}_k\} = \mathbf{H}_k \cdot E\{\mathbf{S}_k\} \quad (1A.10)$$

The covariance matrix of \mathbf{S}_k (representing the correlation between the components of \mathbf{S}_k at the same instant k) is obtained from equation (1A.3) and satisfies the following recursive relation:

$$\text{Cov}\{\mathbf{S}_{k+1}\} = \Phi_k \cdot \text{cov}\{\mathbf{S}_k\} \cdot \Phi_k^T + \mathbf{G}_k \cdot \mathbf{Q}_k \cdot \mathbf{G}_k^T \quad (1A.11)$$

Similarly, the covariance of \mathbf{Z}_k is given by

$$\text{Cov}\{\mathbf{Z}_k\} = \mathbf{H}_k \cdot \text{cov}\{\mathbf{S}_k\} \cdot \mathbf{H}_k^T + \mathbf{L}_k \cdot \mathbf{R}_k \cdot \mathbf{L}_k^T \quad (1A.12)$$

1A.2 Discrete-Time Kalman Filtering

Before describing the Kalman filtering algorithm, it may help to consider an intuitive example of recursive estimation[Bro92]. Consider the problem of estimating the mean of some random constant based on a sequence of noisy measurements. Let us assume that our estimate is to be the sample mean and that we wish to refine our estimate with each new measurement as it becomes available. That is, think of processing the data on-line. Let the measurement sequence be denoted as z_1, z_2, \dots, z_n , where the subscript denotes the time at which the measurement is taken. One method of processing the data would be to store each measurement as it becomes available and then compute the sample mean in accordance with the following algorithm:

First measurement z_1 : Store z_1 and estimate the mean as

$$\hat{m}_1 = z_1 \quad (1A.13)$$

Second measurement z_2 : Store z_2 along with z_1 and estimate the mean as

$$\hat{m}_2 = \frac{z_1 + z_2}{2} \quad (1A.14)$$

Third measurement z_3 : Store z_3 along with z_1 and z_2 and estimate the mean as

$$\hat{m}_3 = \frac{z_1 + z_2 + z_3}{3} \quad (1A.15)$$

And so forth.

Clearly, this would yield the correct sequence of sample means as the experiment progresses. It should also be clear that the amount of memory needed to store the measurements keeps increasing with time, and also the number of arithmetic operations needed to form the estimate increases correspondingly. This would lead to obvious problems when the total amount of data is large. Thus, consider a simple variation in the computational procedure in which each new estimate is formed as a blend of the old estimate and the current measurement. To be specific, consider the following algorithm;

First measurement z_1 : Compute the estimate as

$$\hat{m}_1 = z_1 \quad (1A.16)$$

Store \hat{m}_1 and discard z_1 .

Second measurement z_2 : Compute the estimate as a weighted sum of the previous estimate \hat{m}_1 and the current measurement z_2 :

$$\hat{m}_2 = \frac{1}{2}\hat{m}_1 + \frac{1}{2}z_2 \quad (1A.17)$$

Store \hat{m}_2 and discard z_2 and \hat{m}_1 .

Third measurement z_3 : Compute estimate as a weighted sum of \hat{m}_2 and z_3 :

$$\hat{m}_3 = \frac{2}{3}\hat{m}_2 + \frac{1}{3}z_3 \quad (1A.18)$$

Store \hat{m}_3 and discard z_3 and \hat{m}_2 .

And so forth. It should be obvious that at the k^{th} state the weighted sum is

$$\hat{m}_k = \left(\frac{k-1}{k}\right) \cdot \hat{m}_{k-1} + \left(\frac{1}{k}\right) \cdot z_k \quad (1A.19)$$

Clearly, the above procedure yields the same identical sequence of estimates as before, but without the need to store all the previous measurements. We simply use the result of the previous step to help obtain the estimate at the current step of the process. In this way, the previous computational effort is used to good advantage and not wasted. The second algorithm can proceed on ad infinitum without a growing memory problem. Eventually, of course, as k becomes extremely large, a round-off problem might be encountered. However, this is to be expected with either of the two algorithms.

The second algorithm is a simple example of a recursive mode of operation. The key element in any recursive procedure is the use of the results of the previous step to aid in obtaining the desired result for the current step, and is one of the main features of the Kalman filter.

Now consider the problem of estimating the state \mathbf{S} of a linear, dynamic, discrete-time system from the measurements collected in a finite observation interval, namely $\mathbf{Z}^k = \{\mathbf{Z}_0, \mathbf{Z}_1, \dots, \mathbf{Z}_k\}$. The model assumed for the system is described in equations (2A.4) and (2A.5). The a-priori knowledge about this system consists of the following information:

the initial state \mathbf{S}_0 is a random vector, having known mean value μ_0 and covariance matrix $\mathbf{P}_0 \geq 0$,

the deterministic input \mathbf{U}_k , if present, is known,

the random forcing input $\mathbf{G}_k \cdot \mathbf{V}_k$ is a white noise process, having zero mean and known covariance matrix $\mathbf{Q}_k \geq 0$,

the measurement error process $\mathbf{L}_k \cdot \mathbf{W}_k$ is zero-mean white noise having covariance matrix $\mathbf{R}_k \geq 0$,

the initial state \mathbf{S}_0 is assumed to be uncorrelated with the disturbances $\mathbf{V}_k, \mathbf{W}_k$,

the noise processes $\mathbf{V}_k, \mathbf{W}_k$ are mutually uncorrelated, i.e. $E\{\mathbf{V}_k \cdot \mathbf{W}_k^T\} = \mathbf{0}$.

Two approaches can be followed to derive the Kalman filter equations. The first assumes that the processes $\mathbf{V}_k, \mathbf{W}_k$ and the initial state \mathbf{S}_0 are normally distributed, and the mean square error criterion is then used to obtain an optimum filter which estimates \mathbf{S}_k as $\mathbf{S}^k = E\{\mathbf{S}_k | \mathbf{Z}^k\}$. From the assumptions of a linear model and Gaussian statistics, a linear filter results. The second approach is that of linear minimum mean square error (LMSE), with no assumption on the process distribution functions. It makes use of the following fundamental features of LMSE estimation:

the orthogonality principle between the estimation error and the observations,

the concept of the innovation sequence,

the chance of deriving a recursive updating formula for the estimate when a new measurement becomes available.

From the a-priori knowledge about the process \mathbf{S} , not only the initial value \mathbf{S}_0 can be estimated $\mathbf{S}^0 = \mu_0$ with covariance \mathbf{P}_0 , but also any successive value can be predicted as $\mathbf{S}^k = \mu_k$ from the equation:

$$\mu_{k+1} = \Phi_k \cdot \mu_k + \mathbf{B}_k \cdot \mathbf{U}_k \quad (1A.20)$$

with

$$\mathbf{P}_{k+1} = \Phi_k \cdot \mathbf{P}_k \cdot \Phi_k^T + \mathbf{Q}_k \quad (1A.21)$$

These describe the time evolution of the unconditioned, a-priori mean and covariance of \mathbf{S} . From them it can be observed that, even though the initial guess is very accurate, a prediction error results ($\mathbf{P}^k > \mathbf{0}$) due to the noisy input \mathbf{V}_k . On the other hand, if the initial guess is poor, the prediction error remains severely affected by it for a time depending on the transition matrix Φ_k even if $\mathbf{Q}_k = \mathbf{0}$, i.e. no random input is present.

One potential problem of sequential estimation is termed divergence. The problem occurs when the magnitude of the state vector covariance matrix becomes relatively small. This decrease in $\Delta\mathbf{P}$ occurs naturally as more observations are processed, since the knowledge of the state vector increases with the number of observations processed. When $\Delta\mathbf{P}$ becomes relatively small, the Kalman gain becomes correspondingly small, since $\Delta\mathbf{P}$ is a multiplicative factor in its calculation. The result is that the estimator ignores new data and does not make significant improvements to the state vector. While this would seem to be a desirable result of the estimation process, sometimes $\Delta\mathbf{P}$ becomes artificially small, resulting in the filter disregarding valid observations. To correct this divergence problem, process noise is introduced to limit $\Delta\mathbf{P}$ from below.

We now describe the particular implementation of our model. The measurement vector in Cartesian coordinates is,

$$\mathbf{Z} = \begin{pmatrix} x \\ y \end{pmatrix} \quad (1A.22)$$

and our state vector is,

$$\mathbf{S} = \begin{pmatrix} x \\ \dot{x} \\ y \\ \dot{y} \end{pmatrix} \quad (1A.23)$$

where \dot{x}, \dot{y} represent the velocity of x and y , respectively. The state transition matrix is,

$$\Phi = \begin{pmatrix} 1 & T & 0 & 0 \\ 0 & 1 & 0 & 0 \\ 0 & 0 & 1 & T \\ 0 & 0 & 0 & 1 \end{pmatrix} \quad (1A.24)$$

where T is the scan time of the rotating radar antenna. For simplicity, we assume that the scan time is identical to the time between observations. For a target moving in other than path radial to the radar, the observations will be made at times greater than or less than the scan time, depending on the target velocity and path, and on the antenna rotation direction. We choose a scan time of ten seconds as a reasonable value.

The observation matrix,

$$\mathbf{H} = \begin{pmatrix} 1 & 0 & 0 & 0 \\ 0 & 0 & 1 & 0 \end{pmatrix} \quad (1A.25)$$

simply extracts x and y from the state vector \mathbf{S} so that the state may be compared to the measurements.

The measurement noise, \mathbf{W} , and the process or plant noise, \mathbf{V} , are 2x1 normally distributed vectors with known variance. \mathbf{V} represents the random acceleration of the target, and \mathbf{W} represents random measurement error due primarily to thermal noise in the radar receiver.

\mathbf{L} is a 2x2 identity matrix, which ensures that the measurement noise covariance matrix, \mathbf{R} , is of appropriate dimensions. To model random accelerations in the x and y directions due to model uncertainties, a 4 x 2 matrix, \mathbf{G} , is multiplied by the 2 x 1 vector representing random accelerations, \mathbf{V} , and introduced into the Kalman filter's state estimation calculations. To do this, \mathbf{G} is expressed as

$$\mathbf{G} = \begin{pmatrix} \frac{1}{2}T^2 & 0 \\ T & 0 \\ 0 & \frac{1}{2}T \\ 0 & T \end{pmatrix}. \quad (1A.26)$$

In this way, when \mathbf{G} is multiplied by \mathbf{V} , the random accelerations, the result is in the same dimensions as the state vector. Of course these equations are simply the result of Taylor series expansion of the position, x , with respect to t , expressed in scalar form as,

$$x(t) = x_0 + v \cdot t + \frac{1}{2} \cdot a \cdot t^2 \quad (1A.27)$$

where x_0 is the initial position, v is the velocity, and a is acceleration.

2A. Appendix 2 Derivation of Kalman Filter Equations

2A.1 *First Derivation:*

For simplicity, designate the two independent estimates $s_{k|k-1}^*$ and z_k by s_1^* and s_2^* respectively. Designate $s_{k|k}^*$, the optimum combined estimate, by s_c^* . We desire to find an optimum linear estimate for s_c^* . We can designate this linear estimate as

$$s_c = k_1 \cdot s_1^* + k_2 \cdot s_2^* \quad (2A.1)$$

We want this estimate s_c^* to be unbiased, it being assumed that s_1^* and s_2^* are unbiased. Designate s as the true value of s . Obtaining the mean of (2A.1), it follows that for the estimate to be unbiased

$$s = k_1 \cdot s + k_2 \cdot s \quad (2A.2)$$

which becomes,

$$1 = k_1 + k_2 \quad (2A.3)$$

Thus for the estimate to be unbiased we require,

$$k_2 = 1 - k_1 \quad (2A.4)$$

Substituting (2A.4) into (2A.1) yields,

$$s_c^* = k_1 \cdot s_1^* + (1 - k_1) \cdot s_2^* \quad (2A.5)$$

Let the variances of s_c^* , s_1^* , and s_2^* be designated as σ_c^2 , σ_1^2 , and σ_2^2 . Then (2A.5) yields

$$\sigma_c^2 = k_1^2 \cdot \sigma_1^2 + (1 - k_1)^2 \cdot \sigma_2^2 \quad (2A.6)$$

To find the k_1 that gives the minimum σ_c^2 , we differentiate (2A.6) with respect to k_1 and set the result to zero, obtaining,

$$2 \cdot k_1 \cdot \sigma_1^2 - 2 \cdot (1 - k_1) \cdot \sigma_2^2 = 0 \quad (2A.7)$$

Hence,

$$k_1 = \frac{\sigma_2^2}{\sigma_1^2 + \sigma_2^2} \quad (2A.8)$$

Substituting (2A.8) into (2A.5) yields,

$$s_c^* = \frac{\sigma_2^2}{\sigma_1^2 + \sigma_2^2} \cdot s_1^* + \frac{\sigma_1^2}{\sigma_1^2 + \sigma_2^2} \cdot s_2^* \quad (2A.9)$$

Rewriting (2A.9) yields

$$s_c^* = \left(\frac{s_1^*}{\sigma_1^2} + \frac{s_2^*}{\sigma_2^2} \right) \cdot \frac{1}{\frac{1}{\sigma_1^2} + \frac{1}{\sigma_2^2}} \quad (2A.10)$$

Note that substituting (2A.8) into (2A.6) yields

$$\sigma_c^2 = \left(\frac{1}{\sigma_1^2} + \frac{1}{\sigma_2^2} \right)^{-1} \quad (2A.11)$$

2A.2 Second Derivation:

The second derivation employs a weighted least-squares error estimate approach. In Figure 2A.1 we have two estimates z_k and $s_{k|k-1}^*$ and desire to replace these with a combined estimate $s_{k|k}^*$ that has a minimum weighted least-squares error. For an arbitrarily chosen $s_{k|k}^*$, there are two errors. One is the distance of $s_{k|k}^*$ from z_k ; the other is its distance of $s_{k|k}^*$ from $s_{k|k-1}^*$. For the minimum least-squares

estimate we might minimize the sum of the squares of the distances (errors) between the measurements and the best fitting line (trajectory) to the measurements[Bro98]. We would like to do this in a way that takes into consideration the accuracies of the measurements. For convenience let $s_{k|k-1}^*$ be more accurate than z_k . In this case it is more important that $(s_{k|k-1}^* - s_{k|k}^*)^2$ be small, specifically smaller than $(z_k - s_{k|k}^*)^2$. This would be achieved if in finding the least sum of the squares of each of the two errors we weighted the former error by a larger constant than the latter error. We are thus obtaining a minimization of an appropriately weighted sum of the two errors wherein the former receives a larger weighting. A logical weighting is to weight each term by 1 over the accuracy of their respective estimates as the following equation does:

$$E = \frac{(z_k - s_{k|k}^*)^2}{VAR(z_k)} + \frac{(s_{k|k-1}^* - s_{k|k}^*)^2}{VAR(s_{k|k-1}^*)} \quad (2A.12)$$

Here the error $(s_{k|k-1}^* - s_{k|k}^*)^2$ is weighted by 1 over the variance of $s_{k|k-1}^*$ and $(z_k - s_{k|k}^*)^2$ by 1 over the variance of z_k . Thus if $VAR(s_{k|k-1}^*) \ll VAR(z_k)$, then $1/VAR(s_{k|k-1}^*) \gg 1/VAR(z_k)$ and forces the error $(s_{k|k-1}^* - s_{k|k}^*)^2$ to be much smaller than the error $(z_k - s_{k|k}^*)^2$ when minimizing the weighted sum of the errors in (2A.12). This then forces $s_{k|k}^*$ to be close to $s_{k|k-1}^*$, as it should be. The more accurate $s_{k|k-1}^*$, the closer $s_{k|k}^*$ is to $s_{k|k-1}^*$. In (2A.12) the two errors are automatically weighted according to their importance, the errors being divided by their respective variances. On finding the $s_{k|k}^*$ that minimizes E of (2A.12), a weighted least-squares estimate instead of just a least-squares estimate is obtained. The $s_{k|k}^*$ that minimizes (2A.12) is found by differentiating (2A.12) with respect to $s_{k|k}^*$ and setting the result equal to zero, yielding

$$\frac{\partial E}{\partial s_{k,k}^*} = \frac{2 \cdot (z_k - s_{k|k}^*)}{VAR(z_k)} + \frac{2 \cdot (s_{k|k-1}^* - s_{k|k}^*)}{VAR(s_{k|k-1}^*)} = 0 \quad (2A.13)$$

Solving (2A.13) yields

$$s_{k,k}^* = \left[\frac{s_{k|k-1}^*}{VAR(s_{k|k-1}^*)} + \frac{z_k}{VAR(z_k)} \right] \cdot \frac{1}{\frac{1}{VAR(s_{k|k-1}^*)} + \frac{1}{VAR(z_k)}} \quad (2A.14)$$

Now let us extend this derivation to the case of vector measurements and states. As done for the one-dimensional case, we weight the square of the errors by 1 over the variance of the error. Thus our error (or cost) function as in (2A.12) now denoted as \mathbf{J} is as follows,

$$\mathbf{J} = \frac{(\mathbf{Z}_k - \mathbf{S}_{k|k}^*)^2}{VAR(\mathbf{Z}_k)} + \frac{(\mathbf{S}_{k|k-1}^* - \mathbf{S}_{k|k}^*)^2}{VAR(\mathbf{S}_{k|k-1}^*)} \quad (2A.15)$$

Of course this equation is only conceptually correct; the mathematically correct equivalent will be given shortly.

Now we will use (2A.15) to solve for the new combined estimate $\mathbf{S}_{k|k}^*$ that minimizes the weighted sum of the squares of the errors. Conceptually, this is done just as it was done for the equivalent one-dimensional (2A.12). Specifically, (2A.15) is differentiated with respect to the combined estimate $\mathbf{S}_{k|k}^*$ with the resulting equation set equal to zero in order to solve for the combined estimate $\mathbf{S}_{k|k}^*$ that minimizes the weighted sum of the errors squared. Note that (2A.15) is not mathematically correct when operating on matrices, as will be shown.

When using matrix notation, the first term on the right of the equal sign in (2A.15) must be written as

$$\frac{(\mathbf{Z}_k - \mathbf{S}_{k|k}^*)^2}{VAR(\mathbf{Z}_k)} \equiv (\mathbf{Z}_k - \mathbf{S}_{k|k}^*)^T \cdot \mathbf{R}_k^{-1} \cdot (\mathbf{Z}_k - \mathbf{S}_{k|k}^*) \quad (2A.16)$$

Where the matrix \mathbf{R}_k is the covariance matrix of \mathbf{Z}_k , that is,

$$\mathbf{R}_k = \text{COV}(\mathbf{Z}_k) \quad (2A.17)$$

The inverse of the covariance matrix \mathbf{R}_k , which is designated as \mathbf{R}_k^{-1} , takes the place of dividing by the variance of \mathbf{Z}_k when dealing with matrices. The corresponding correct form for the second term on the right of (2A.15) is

$$\frac{(\mathbf{S}_{k|k-1}^* - \mathbf{S}_{k|k}^*)^2}{\text{VAR}(\mathbf{Z}_k)} \equiv (\mathbf{S}_{k|k-1}^* - \mathbf{S}_{k|k}^*)^T \cdot \mathbf{P}_{k|k-1}^{*-1} \cdot (\mathbf{S}_{k|k-1}^* - \mathbf{S}_{k|k}^*) \quad (2A.18)$$

Where $\mathbf{P}_{k|k-1}^*$ is the covariance matrix of $\mathbf{S}_{k|k-1}^*$. Substituting (2A.17) and (2A.18) into (2A.15) yields

$$\mathbf{J} = (\mathbf{Z}_k - \mathbf{H} \cdot \mathbf{S}_{k|k}^*)^T \mathbf{R}_k^{-1} (\mathbf{Z}_k - \mathbf{H} \cdot \mathbf{S}_{k|k}^*) + (\mathbf{S}_{k|k-1}^* - \mathbf{S}_{k|k}^*)^T \mathbf{P}_{k|k-1}^{*-1} (\mathbf{S}_{k|k-1}^* - \mathbf{S}_{k|k}^*) \quad (2A.19)$$

Now we may solve for the optimal $\mathbf{S}_{k|k}^*$ as we did in the scalar case, by differentiating the error function \mathbf{J} with respect to $\mathbf{S}_{k|k}^*$, setting the equation equal to zero and solving for $\mathbf{S}_{k|k}^*$. Differentiation of a matrix equation is achieved by obtaining the gradient of the matrix equation as given by

$$\text{Gradient of } \mathbf{J} \equiv \frac{\partial \mathbf{J}}{\partial \mathbf{S}_{k|k}^*} = \left[\frac{\partial \mathbf{J}}{\partial s_1}, \frac{\partial \mathbf{J}}{\partial s_2}, \dots, \frac{\partial \mathbf{J}}{\partial s_n} \right] \quad (2A.20)$$

Applying (2A.20) to (2A.19) yields

$$\frac{\partial \mathbf{J}}{\partial \mathbf{S}_{k,k}^*} = 2 \cdot (\mathbf{S}_{k,k}^* - \mathbf{S}_{k,k-1}^*)^T \cdot \mathbf{P}_{k,k-1}^{*-1} + 2(\mathbf{Z}_k - \mathbf{H} \cdot \mathbf{S}_{k,k}^*)^T \cdot \mathbf{R}_k^{-1} \cdot (-\mathbf{H}) = 0 \quad (2A.21)$$

Where \mathbf{H} is the observation matrix which (in our case) merely extracts the measurement estimates from \mathbf{S} . Equation (2A.21) can be rewritten as

$$\mathbf{S}_{k|k}^{*T} \cdot (\mathbf{P}_{k|k}^{*-1} + \mathbf{H}^T \cdot \mathbf{R}_k^{-1} \cdot \mathbf{H}) = \mathbf{S}_{k|k-1}^{*T} \cdot \mathbf{P}_{k|k-1}^{*-1} + \mathbf{Z}_k^T \cdot \mathbf{R}_k^{-1} \cdot \mathbf{H} \quad (2A.22)$$

Which on taking the transpose of both sides and using the identity $(\mathbf{AB})^T = \mathbf{B}^T \mathbf{A}^T$ yields

$$(\mathbf{P}_{k|k}^{*-1} + \mathbf{H}^T \cdot \mathbf{R}_k^{-1} \cdot \mathbf{H}) \cdot \mathbf{S}_{k|k}^* = \mathbf{P}_{k|k-1}^{*-1} \cdot \mathbf{S}_{k|k-1}^* + \mathbf{H}^T \cdot \mathbf{R}_k^{-1} \cdot \mathbf{Z}_k \quad (2A.23)$$

or,

$$\mathbf{S}_{k|k}^* = (\mathbf{P}_{k|k-1}^{*-1} + \mathbf{H}^T \cdot \mathbf{R}_k^{-1} \cdot \mathbf{H})^{-1} \cdot (\mathbf{P}_{k|k-1}^{*-1} \cdot \mathbf{S}_{k|k-1}^* + \mathbf{H}^T \cdot \mathbf{R}_k^{-1} \cdot \mathbf{Z}_k) \quad (2A.24)$$

Applying the well-known matrix inversion lemma,

$$(\mathbf{P}_{k|k}^{*-1} + \mathbf{H}^T \cdot \mathbf{R}_k^{-1} \cdot \mathbf{H})^{-1} = \mathbf{P}_{k|k-1}^* - \mathbf{P}_{k|k-1}^* \cdot \mathbf{H}^T \cdot (\mathbf{R}_k + \mathbf{H} \cdot \mathbf{P}_{k|k-1}^* \cdot \mathbf{H}^T)^{-1} \cdot \mathbf{H} \cdot \mathbf{P}_{k|k-1}^* \quad (2A.25)$$

This can be rewritten as

$$(\mathbf{P}_{k|k}^{*-1} + \mathbf{H}^T \cdot \mathbf{R}_k^{-1} \cdot \mathbf{H})^{-1} = \mathbf{P}_{k|k-1}^* - \mathbf{K}_k \cdot \mathbf{H} \cdot \mathbf{P}_{k|k-1}^* \quad (2A.26)$$

where \mathbf{K}_k is often called the Kalman gain and is given by,

$$\mathbf{K}_k = \mathbf{P}_{k|k-1}^* \cdot \mathbf{H}^T \cdot (\mathbf{R}_k + \mathbf{H} \cdot \mathbf{P}_{k|k-1}^* \cdot \mathbf{H}^T)^{-1} \quad (2A.27)$$

Substituting (2A.26) into (2A.24) yields

$$\begin{aligned} \mathbf{S}_{k|k}^* &= (\mathbf{P}_{k|k-1}^{*-1} - \mathbf{K}_k \cdot \mathbf{H} \cdot \mathbf{P}_{k|k-1}^*)^{-1} \cdot (\mathbf{P}_{k|k-1}^{*-1} \cdot \mathbf{S}_{k|k-1}^* + \mathbf{H}^T \cdot \mathbf{R}_k^{-1} \cdot \mathbf{Z}_k) \\ &= \mathbf{S}_{k|k-1}^* - \mathbf{K}_k \cdot \mathbf{H} \cdot \mathbf{S}_{k|k-1}^* + (\mathbf{P}_{k|k-1}^* - \mathbf{K}_k \cdot \mathbf{H} \cdot \mathbf{P}_{k|k-1}^*) \cdot \mathbf{H}^T \cdot \mathbf{R}_k^{-1} \cdot \mathbf{Z}_k \end{aligned} \quad (2A.28)$$

But as will be shown shortly,

$$\mathbf{K}_k = (\mathbf{P}_{k|k-1}^* - \mathbf{K}_k \cdot \mathbf{H} \cdot \mathbf{P}_{k|k-1}^*) \cdot \mathbf{H}^T \cdot \mathbf{R}_k^{-1} \quad (2A.29)$$

Then (2A.28) can be rewritten as

$$\mathbf{S}_{k|k}^* = \mathbf{S}_{k|k-1}^* + \mathbf{K}_k \cdot \mathbf{Z}_k - \mathbf{K}_k \cdot \mathbf{H} \cdot \mathbf{S}_{k|k-1}^* \quad (2A.27)$$

or

$$\mathbf{S}_{k|k}^* = \mathbf{S}_{k|k-1}^* + \mathbf{K}_k \cdot (\mathbf{Z}_k - \mathbf{H} \cdot \mathbf{S}_{k|k-1}^*) \quad (2A.28)$$

Now we can prove (2A.29). From (2A.27) it follows that

$$\mathbf{P}_{k|k-1}^* \cdot \mathbf{H}^T = \mathbf{K}_k \cdot (\mathbf{R}_k + \mathbf{H} \cdot \mathbf{P}_{k|k-1}^* \cdot \mathbf{H}^T) \quad (2A.29)$$

Finishing the proof, this equation can be written as

$$\mathbf{P}_{k|k-1}^* \cdot \mathbf{H}^T \cdot \mathbf{R}_k^{-1} - \mathbf{K}_k \cdot \mathbf{H} \cdot \mathbf{P}_{k|k-1}^* \cdot \mathbf{H}^T \cdot \mathbf{R}_k^{-1} = \mathbf{K}_k \quad (2A.30)$$

3A. Appendix 3 Local to Global Coordinate Transformation

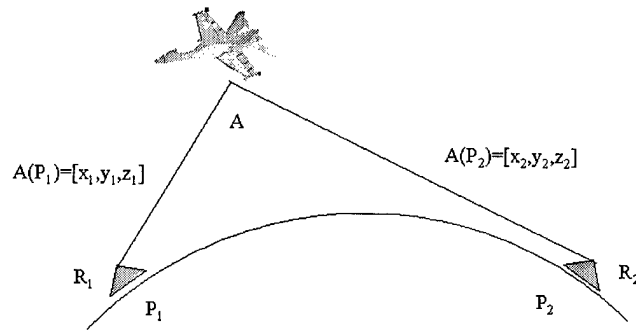


Figure 3A-1 Target in two Radar System

Let the radars R_1 and R_2 be situated at points P_1 and P_2 on the earth's surface as shown in Figure 3A-1. An airplane A is detected by the radar R_1 in its local Cartesian coordinate system \mathbf{P}_1 with the coordinates $[x_1, y_1, z_1] \equiv A(\mathbf{P}_1)$, and it is necessary to find the coordinates $[x_2, y_2, z_2] \equiv A(\mathbf{P}_2)$ of the airplane A in the Cartesian coordinate system \mathbf{P}_2 of the radar R_2 . The points P_1, P_2 are given by the geographical coordinates $[f_1, l_1]$ and $[f_2, l_2]$, where f_1, f_2 are the geographical latitudes and l_1, l_2 are the geographical longitudes. The x_1 - y_1 plane is tangent to the ellipsoid at the point P_1 . The x_1 axis lies in the plane of the latitude f_1 , the y_1 axis lies in the plane of the meridian l_1 . The z_1 axis is positively oriented towards the earth's center. The x_1 axis and the y_1 axis are oriented in the direction of increasing longitude and latitude, respectively. The axes of the coordinate system \mathbf{P}_2 are similarly oriented.

Next it is desired to transform the geographical coordinates $[f, l]$ of a point P into geocentric Cartesian coordinates $(C; x_c, y_c, z_c) \equiv \mathbf{C}$, with origin C at the earth's center as seen in Figure 3A-2. The z_c axis goes through the earth's poles, with the positive orientation to the North Pole. The x_c axis passes through the null and 180^{th} meridian, the positive orientation to the null meridian. The y_c axis is perpendicular to the x_c axis and to the z_c axis, with positive orientation to the 90^{th} meridian.

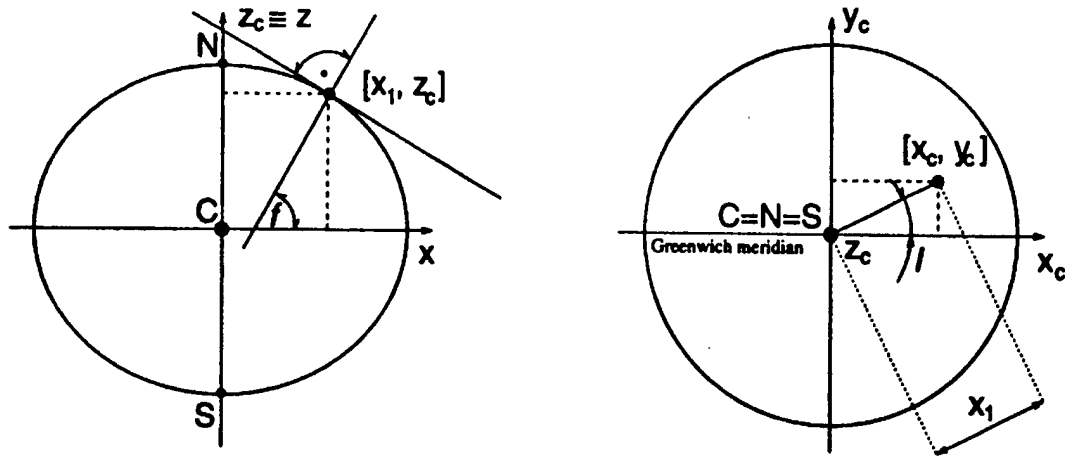


Figure 3A-2 Transformation from Geographical to Geocentric Coordinates

The shape of the Earth is a geoid, however for simplicity, an ellipsoid will be used as an approximation, see Figure 3A-3. Denote the major semi-axis as $A = 6378.245$ [km] and the minor semi-axis $B = 6356.863$ [km]. To derive the transformation equations it is convenient to use the parametric description of the ellipse. The usual parametric representation of the ellipse is

$$x(\varphi) = A \cos(\varphi), \quad z(\varphi) = B \sin(\varphi) \quad (3A.1)$$

In order to relate the angle f to x and z we must first compute the normal vector \vec{n} at $[x, z]$

$$\vec{t} \equiv \begin{pmatrix} \dot{x} \\ \dot{z} \end{pmatrix} = \begin{pmatrix} -A \sin(\varphi) \\ B \cos(\varphi) \end{pmatrix} \Rightarrow \vec{n} \equiv \begin{pmatrix} -\dot{z} \\ \dot{x} \end{pmatrix} = \begin{pmatrix} -B \cos(\varphi) \\ -A \sin(\varphi) \end{pmatrix} \quad (3A.2)$$

Therefore,

$$\tan(f) = -\frac{\dot{x}}{\dot{z}} = \frac{A}{B} \tan(\varphi). \quad (3A.3)$$

From $\tan(\varphi) = \frac{B}{A} \tan(f)$ we can obtain,

$$\cos(\varphi) = \frac{1}{\sqrt{1 + \tan^2(\varphi)}}, \sin(\varphi) = \tan(\varphi) \cos(\varphi) \quad (3A.4)$$

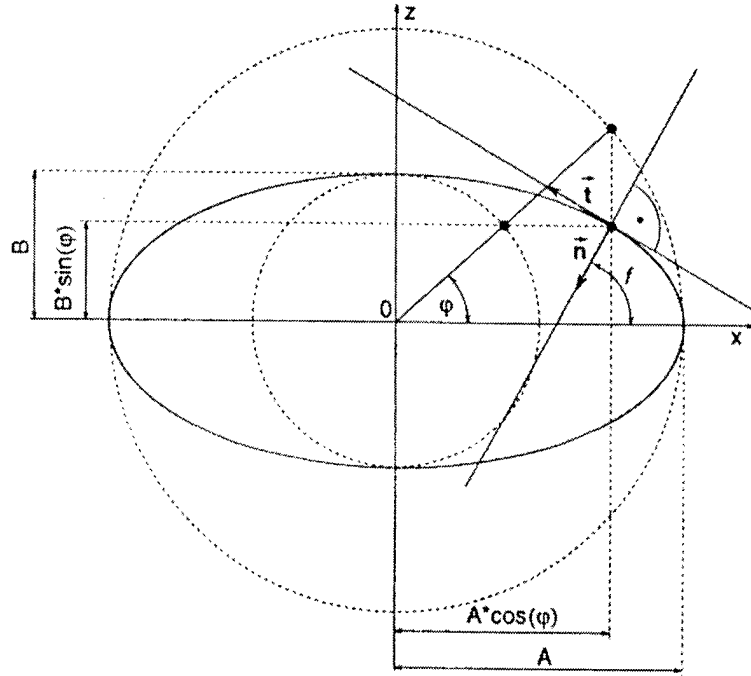


Figure 3A-3 An Ellipse Description by the Slope of the Normal Vector

Now the transformation from the coordinate system \mathbf{P}_1 in to the coordinate system \mathbf{P}_2 can be performed, see Figure 3A-4. This transformation consists of four partial transformations, more precisely, one translation and three rotations. Since the coordinate system \mathbf{P}_1 changes after each transformation, we must distinguish the coordinate systems using a superscript:

$$\mathbf{P}_1^i, i = 0, \dots, 4, ; \mathbf{P}_1^0 \equiv \mathbf{P}_1, \mathbf{P}_1^4 \equiv \mathbf{P}_2 \quad (3A.5)$$

3A.1 The Translation:



$\bar{\Delta}p(C) = P_2(C) - P_1(C)$. Now we need to transform $\bar{\Delta}p(C)$ into $\bar{\Delta}p(P_I)$. This transformation can be computed as follows.

First, we must place the origin P_1'' of the coordinate system \mathbf{P}_1'' at the intersection of the equator and the Greenwich meridian. This transformation is:

70

To move P_1'' into P_1' , we perform a rotation around the y'' axis with the angle l_1 . This transformation can be described by the rotation matrix R_1 .

$$\begin{pmatrix} \Delta x \\ \Delta y \\ \Delta z \end{pmatrix}_{P_1'} = R_1 \times \begin{pmatrix} \Delta x \\ \Delta y \\ \Delta z \end{pmatrix}_{P_1''}, R_1 = \begin{pmatrix} \cos(l_1) & 0 & \sin(l_1) \\ 0 & 1 & 0 \\ -\sin(l_1) & 0 & \cos(l_1) \end{pmatrix}. \quad (3A.7)$$

To move P_1' into P_1 , we use a rotation around the x' axis with the angle f_1 . This transformation is described by the matrix R_2 :

$$\begin{pmatrix} \Delta x \\ \Delta y \\ \Delta z \end{pmatrix}_{P_1} = R_2 \times \begin{pmatrix} \Delta x \\ \Delta y \\ \Delta z \end{pmatrix}_{P_1'}, R_2 = \begin{pmatrix} 1 & 0 & 0 \\ 0 & \cos(f_1) & \sin(f_1) \\ 0 & -\sin(f_1) & \cos(f_1) \end{pmatrix}. \quad (3A.8)$$

Now the coordinate system P_1 is in a general position. Summarizing the previous steps, the translation vector $\bar{\Delta p}(P_1)$ can be expressed by

$$\begin{pmatrix} \Delta x \\ \Delta y \\ \Delta z \end{pmatrix}_{P_1} = R_2 \times R_1 \times M \times \begin{pmatrix} P_{2x} - P_{1x} \\ P_{2y} - P_{1y} \\ P_{2z} - P_{1z} \end{pmatrix}_C. \quad (3A.9)$$

The new coordinates $A(P_1^I)$ can be obtained from the previous coordinates $A(P_1)$ by using the relation

$$A(P_1^I) \equiv \begin{pmatrix} x \\ y \\ z \end{pmatrix}_{P_1^I} = A(P_1) - \begin{pmatrix} \Delta x \\ \Delta y \\ \Delta z \end{pmatrix}_{P_1}. \quad (3A.10)$$

3A.2 First Rotation:

We rotate the \mathbf{P}_1^1 coordinate system around the x axes by the angle f_1 in order to make the y axis parallel to the earth axis z_c . Then, the new coordinates of the airplane $A(\mathbf{P}_1^2)$ are obtained from the previous coordinates $A(\mathbf{P}_1^1)$ using

$$A(\mathbf{P}_1^2) \equiv \begin{pmatrix} x \\ y \\ z \end{pmatrix}_{P_1^2} = R_3 \times \begin{pmatrix} x \\ y \\ z \end{pmatrix}_{P_1^1}, R_3 = R_2^T \equiv \begin{pmatrix} 1 & 0 & 0 \\ 0 & \cos(f_1) & -\sin(f_1) \\ 0 & \sin(f_1) & \cos(f_1) \end{pmatrix}. \quad (3A.11)$$

3A.3 Second Rotation:

We rotate the \mathbf{P}_1^2 coordinate system by the angle $\Delta l = l_2 - l_1$ around the y axis in order to let the two x axes of \mathbf{P}_1^2 and \mathbf{P}_2 coincide. The new coordinates $A(\mathbf{P}_1^3)$ of the airplane are then computed from the previous coordinates $A(\mathbf{P}_1^2)$ by

$$A(\mathbf{P}_1^3) \equiv \begin{pmatrix} x \\ y \\ z \end{pmatrix}_{P_1^3} = R_4 \times \begin{pmatrix} x \\ y \\ z \end{pmatrix}_{P_1^2}, R_4 \equiv \begin{pmatrix} \cos(\Delta l) & 0 & \sin(\Delta l) \\ 0 & 1 & 0 \\ -\sin(\Delta l) & 0 & \cos(\Delta l) \end{pmatrix}. \quad (3A.12)$$

3A.4 Third Rotation:

We rotate the system \mathbf{P}_1^3 by the angle f_2 around the x axis to let it coincide with the system \mathbf{P}_2 . Thus, the final coordinates $A(\mathbf{P}_2) \equiv A(\mathbf{P}_1^4)$ of the airplane A are obtained from the previous coordinates $A(\mathbf{P}_1^3)$ by

$$A(\mathbf{P}_2) \equiv \begin{pmatrix} x \\ y \\ z \end{pmatrix}_{P_1^4} = R_5 \times \begin{pmatrix} x \\ y \\ z \end{pmatrix}_{P_1^3}, R_5 \equiv \begin{pmatrix} 1 & 0 & 0 \\ 0 & \cos(f_2) & \sin(f_2) \\ 0 & -\sin(f_2) & \cos(f_2) \end{pmatrix}. \quad (3A.13)$$

The above steps can be combined by concatenation. By using matrices $R_1 - R_5$ we get the overall transformation

$$A(\mathbf{P}_2) \equiv \begin{pmatrix} x \\ y \\ z \end{pmatrix}_{P_2} = R_5 \times R_4 \times R_2^T \times \left(A(\mathbf{P}_1) - R_2 \times R_1 \times M \times \begin{pmatrix} P_{2x} - P_{1x} \\ P_{2y} - P_{1y} \\ P_{2z} - P_{1z} \end{pmatrix}_C \right). \quad (3A.14)$$

3A.5 MatLab Routines

The following two MatLab functions are (1) the S-function used for calling the algorithm that performs the above calculations, and (2) the actual function that performs the algorithm.

```
function [sys,x0,str,ts] = s_change_view(t,x,u,flag)
switch flag,
    %%%%%%%%%%%%%%%
    % Initialization %
    %%%%%%%%%%%%%%%
    case 0,
        [sys,x0,str,ts] = mdlInitializeSizes;
        %%%%%%%%%%%%%%%
    % Update %
    %%%%%%%%%%%%%%%
    %case 2,
    % sys = mdlUpdate;
    %%%%%%%%%%%%%%%
    % Output %
    %%%%%%%%%%%%%%%
    case 3,
        sys = mdlOutputs(t,x,u);
        %%%%%%%%%%%%%%%
    % Terminate %
    %%%%%%%%%%%%%%%
    case {1,2,4,9},
        sys = []; % do nothing
        %%%%%%%%%%%%%%%
    % Unexpected flags %
    %%%%%%%%%%%%%%%
    otherwise
        error(['unhandled flag = ',num2str(flag)]);
end
%end dsfunc
%
%=====
% mdlInitializeSizes
% Return the sizes, initial conditions, and sample times for the S-function.
%=====
%
```

```
function [sys,x0,str,ts] = mdlInitializeSizes
```

```

sizes = simsizes;
sizes.NumContStates = 0;
sizes.NumDiscStates = 0;
sizes.NumOutputs = 3;
sizes.NumInputs = -1;
sizes.DirFeedthrough = 1;
sizes.NumSampleTimes = 1;
sys = simsizes(sizes);
x0 = [];
str = [];
ts = [-1 0];
%=====
% mdlUpdate
% Handle discrete state updates, sample time hits, and major time step
% requirements.
%=====
%
%=====
% mdlOutputs
% Return the output vector for the S-function
%=====
function sys = mdlOutputs(t,x,u)
%function[A2]=transf(lat1,lon1,A1,lat2,lon2)
%lat1-2,lon1-2 = geographical radar positions in (radians)
%A1=[x;y;z],(P1)=position of airplane seen by radar at P1
%A2=position of airplane seen by radar at P2
sys=transf(u(1),u(2),u(3:5),u(6),u(7));

%sys=transf(lat1,lon1,(x,y,z)of target,lat2,lon2)
%sys is [x;y;z] position of target seen by radar2 at lat2,lon2
function[A2]=transf(lat_1,lon_1,A_1,lat_2,lon_2)
%lat1-2,lon1-2 = geographical radar positions in (degrees)
%A1=[x;y;z],(P1)=position of airplane seen by radar at P1
lat1=deg2rad(lat_1);
lon1=deg2rad(lon_1);
lat2=deg2rad(lat_2);
lon2=deg2rad(lon_2);
A1=A_1;
M=[0 1 0;
    0 0 1;
    -1 0 0];
R1=[cos(lon1) 0 sin(lon1);
    0 1 0;
    -sin(lon1) 0 cos(lon1)];
R2=[1 0 0;0 cos(lat1) sin(lat1);0 -sin(lat1) cos(lat1)];
P1c=gg2gc(lat1,lon1);
P2c=gg2gc(lat2,lon2);

```

```

DPc=P2c-P1c;
T=R2*R1*M*DPc;
a=A1-T;
D1=lon2-lon1;
R4=[cos(D1) 0 sin(D1);
    0 1 0;
    -sin(D1) 0 cos(D1)];
R5=[1 0 0;
    0 cos(lat2) sin(lat2);
    0 -sin(lat2) cos(lat2)];
A2=R5*R4*R2'*a; %position of airplane seen by radar at P2

```

4A. Appendix 4 Modified Munkres Algorithm

% Modified Munkres Optimal assignment algorithm, rows=tracks, cols=observations

function [x_ret,cov_file_ret,z_file_ret]=munkres(x)

[nrows,ncols]=size(x);

k=min(nrows,ncols);

z_file=randint(nrows,ncols,80:90);

z_file=char(z_file);

cov_file=z_file;

% Preliminaries: if $m > n$, for each column subtract min(column) from that column

% if $n > m$, for each row subtract min(row) from that row

if nrows>ncols,

for I=1:ncols,

x(:,I)=x(:,I)-min(x(:,I));

m(I)=find(x(:,I)==0);

end;

[x_ret,cov_file_ret,z_file_ret]=munk_1(x,cov_file,z_file);

else;

for I=1:nrows,

x(I,:)=x(I,:)-min(x(I,:));

n(I)=find(x(I,:)==0);

end

[x_ret,cov_file_ret,z_file_ret]=munk_1(x,cov_file,z_file);

end

%----- Step 1 -----

function [x_ret,cov_file_ret,z_file_ret]=munk_1(x,cov_file,z_file)

[j,k]=find(x(:,:)==0);

for p=1:length(j),% for all 0's, if no 0* in row or column of 0, star the 0

if length(find(z_file(j(p),:)=='*'))==0 & length(find(z_file(:,k(p))=='*'))==0,

z_file(j(p),k(p))='*';

end

end

if ~exist('x_ret')

[x_ret,cov_file_ret,z_file_ret]=munk_2(x,cov_file,z_file);

end

%----- Step 2 -----

function [x_ret,cov_file_ret,z_file_ret]=munk_2(x,cov_file,z_file)

if exist('x_ret')

else

while length(find(any(z_file=='*')==1))< min(size(x))& ~exist('x_ret'), %go until final solution

[j,k]=find(z_file(:,:)=='*');

for I=1:length(k),

cov_file(:,k(I))='c';

end

[x_ret,cov_file_ret,z_file_ret]=munk_3(x,cov_file,z_file);

```

end

    if length(find(any(z_file=='')==1))== min(size(x)) & ~exist('x_ret'),
        %x_ret=x;
        x_ret=[];
        %cov_file_ret=cov_file;
        cov_file_ret=[];
        z_file_ret=z_file;
    end;
end

%-----Step 3-----
function [x_ret,cov_file_ret,z_file_ret]=munk_3(x,cov_file,z_file)
if length(find(any(z_file=='')==1))== min(size(x)) & ~exist('x_ret')
    x_ret=x;
    cov_file_ret=cov_file;
    z_file_ret=z_file;
else

[j,k]=find(x(:,.)==0 & cov_file(:,.)~='c' & z_file(:,.)~='*' & z_file(:,.)~='');
% find uncovered zeros
for zz=1:length(j),
    if length(j)>0 & length(find(any(z_file=='')==1))< min(size(x));
        z_file(j(zz),k(zz))=''; % Pick uncovered Z and prime it to Z'
        if length(find(z_file(j(zz),:)=='*'))>=1 ; %if there is a 0* in this row
            %z_file(j(zz),k(zz))='';
            b=find(z_file(j(zz),:)=='*');
            cov_file(:,b)='u'; % uncover col of Z'
            cov_file(j(zz),:)= 'c'; % cover row of Z'
        elseif length(find(z_file(j(zz),:)=='*'))==0; % if no Z* in in row of Z' do step 4
            [x_ret,cov_file_ret,z_file_ret]=munk_4(x,cov_file,z_file)
        end
        if exist('x_ret')
            break
        end
    end
end
[j,k]=find(x(:,.)==0 & cov_file(:,.)~='c' & z_file(:,.)~='*' & z_file(:,.)~='');
end
    if length(find(any(z_file=='')==1))< min(size(x)) & ~exist('x_ret')
        [x_ret,cov_file_ret,z_file_ret]=munk_5(x,cov_file,z_file);
    end
end

%-----% Step 4-----
function [x_ret,cov_file_ret,z_file_ret]=munk_4(x,cov_file,z_file)%Step 4
%z_file_seq=z_file;% temp file to record sequence of z', z*, etc

if length(find(any(z_file=='')==1))== min(size(x)) & ~exist('x_ret')
    x_ret=[];%x;
    cov_file_ret=[];%cov_file;
    z_file_ret=z_file;
else

```

```

[u,v]=find(z_file(:,:)==' ' & cov_file(:,:)=='c');% find the uncovered Z'
uu=find(z_file(:,v)=='*');
if isempty(uu),
    z_file(u,v)=='*';
else
    z_file(u,v)=='*';% Star the Z' with a Z* in its column
    z_file(uu,v)==' '; % Un-star the Z* in that column
    while ~isempty(uu), % while any Z* in col of Z', Z' in row of Z*, etc
        vv=find(z_file(uu,:)==' ');% Find Z' in row of un-starred Z*
        if ~isempty(vv)% If there is a Z' in row of un-starred Z*
            z_file(uu,vv)==' '; % Star the Z'
            uu=find(z_file(:,vv)=='*');% Find Z* in col of Z'
            if ~isempty(uu)% if there is a Z*
                z_file(uu,vv)==' ';% Blank it out
            end
        end
    end
    uu=[];
end
end
end
z_file(find(z_file(:,:)==' '))=='*';% Star all Z' from sequence
z_file(find(z_file(:,:)==' '))==' ';% Erase all Primes from Z'
cov_file(find(cov_file(:,:)=='u'))=='c'; % Uncover all covered rows/cols
if length(find(any(z_file=='*')==1))== min(size(x)) & ~exist('x_ret')
    x_ret=[];%x;
    cov_file_ret=[];%cov_file;
    z_file_ret=z_file;
else
    [x_ret,cov_file_ret,z_file_ret]=munk_2(x,cov_file,z_file);
end
end
% Modified Munkres Optimal assignment algorithm, rows=tracks, cols=observations

%----- Munkres Algorithm Step 5-----
function [x_ret,cov_file_ret,z_file_ret]=munk_5(x,cov_file,z_file)
if length(find(any(z_file=='*')==1))== min(size(x))
    x_ret=x;
    cov_file_ret=cov_file;
    z_file_ret=z_file;
else
    h=min(x(find(cov_file(:,:)=='c')));
    i=all(cov_file=='c',2);%find covered row
    i=find(i==1);% # of covered rows
    if length(i)>0 & length(find(any(z_file=='*')==1))< min(size(x));
        for I=1:length(i),
            x(i(I,:))=x(i(I,:))+h;% add h to covered rows
        end
    end
end
z=find(z==1);
if length(z)>0 & length(find(any(z_file=='*')==1))< min(size(x));

```

```

    for I=1:length(z),
        x(:,z(I))=x(:,z(I))-h;
    end
% go back to step 3
[j,k]=find(x(:,:)==0 & cov_file(:,:)'~='c'); % find uncovered zeros
end
[x_ret,cov_file_ret,z_file_ret]=munk_3(x,cov_file,z_file);
end

```


6. List of Notation / Symbols

B,G,L	matrices in dynamic system model that account for measurement and model uncertainties
H	observation matrix, (extracts measurement variables from state vector S)
Φ	state transition matrix
$E\{.\}$	expectation operator
$E\{x z\}$	conditional expectation of x given z
K_k	Kalman gain matrix at time k
P	covariance matrix
\hat{P}	estimation covariance matrix
$\hat{P}_{k k}, \hat{P}_{k k-1}$	covariance matrix of filtered and predicted estimates, respectively
Q,R	process covariance, and measurement covariance matrices, respectively
S_k	system state at the k^{th} time instant
$\hat{S}_{k k}$	filtered estimate of S_k
$\hat{S}_{k k-1}$	predicted estimate of S_k
Z	vector of measurements
v_k	innovation process at time k
Θ_k	covariance matrix of the innovation

7. Bibliography

- [Bar90] Bar Shalom, Y., editor, *Multitarget-Multisensor Tracking: Advanced Applications*, Artech House, Norwood, MA, 1990.
- [Bla86] Blackman, S., *Multiple-Target Tracking with Radar Applications*, Artech House, Dedham, MA, 1986.
- [Bog90] Bogler, P., *Radar Principles with Applications to Tracking Systems*, John Wiley & Sons, New York, 1990.
- [Bro92] Brown, G., and Hwang, P., *Introduction to Random Signals and Applied Kalman Filtering*, John Wiley & Sons, New York, 1990.
- [Bro98] Brookner, E., *Tracking and Kalman Filtering Made Easy*, John Wiley & Sons, New York, 1998.
- [Fa185] Farina, S., and Studer, F.A., *Radar Data Processing-Vol. I Introduction and Tracking*, Research Studies Press Ltd., New York, 1985.
- [Fa285] Farina, S., and Studer, F.A., *Radar Data Processing-Vol. II Advanced Topics and Applications*, Research Studies Press Ltd., New York, 1985.
- [Hal92] Hall, D., *Mathematical Techniques in Multisensor Data Fusion*, Artech House, Norwood, MA, 1992.
- [Sko90] Skolnik, M., Editor in Chief, *Radar Handbook, 2nd Edition*, McGraw-Hill, New York, 1990.
- [Spi97] Spiegel, M., *Schaum's Outline of Theory and Problems of Probability and Statistics*, McGraw-Hill, New York, 1997.

8. Vita

Captain Bradley John Mortenson was born December 7, 1964 in Amery, Wisconsin. He was raised in Polk County, Wisconsin, and graduated from St. Croix Falls High School in 1983. Mortenson enlisted in the USAF in 1986 and was assigned to the 7th Munitions Maintenance Squadron at Carswell AFB, Texas where he maintained air-launched cruise, and short-range attack missiles. After separating as a Sergeant in 1990, Mortenson attended the University of Texas at Arlington, where he received a Bachelor of Science in Electrical Engineering in 1992. Captain Mortenson was commissioned in the United States Air Force via Officer's Training School in November, 1994 as a distinguished graduate. His first assignment as an officer was as a B-2A Research Engineer with the 509th Logistics Support Squadron at Whiteman Air Force Base, Missouri. From Whiteman, Mortenson went on to the Air Force Institute of Technology in Dayton, Ohio to pursue a Master's of Science in Electrical Engineering. His subsequent assignment was to the National Air Intelligence Center at Wright Patterson AFB, Ohio.

Permanent Address:

1933 75th Ave.
Dresser, WI 54009